A&A 378, 327–344 (2001)
DOI: 10.1051/0004-6361:20011166

Astronomy & Astrophysics

RFI mitigation methods in radio astronomy

P. A. Fridman and W. A. Baan

ASTRON, Netherlands Foundation for Research in Astronomy, and Westerbork Observatory, Postbus 2, 7990AA Dwingeloo, The Netherlands

Received 8 June 2001 / Accepted 20 August 2001

Abstract. Various methods of radio frequency interference (*RFI*) mitigation methods at radio astronomy telescopes are being considered. Special attention is given to real-time processing algorithms. Computer simulations and observational results are used to describe the applicability of these methods. Best results can be achieved when the *RFI* mitigation procedures are adapted to the particular radio telescope, the type of observations, and the peculiarities of the *RFI* environment. A combination of different linear and non-linear methods in the temporal and frequency domains, with and without the use of reference antennas, may give considerable suppression of strong *RFI*.

Key words. techniques: interferometric, miscellaneous – methods: statistical, numerical, miscellaneous

1. Introduction

Radio astronomy uses the radio spectrum to detect weak emissions from celestial sources. The frequencies at which these emissions can be seen are completely determined by the physical processes occurring at the site of origin. Generally speaking, the whole electro-magnetic spectrum contains information on the physics of celestial sources. Improvements in antenna quality and receiver parameters seek to lower the detection levels for these sources at all available frequencies. However, the real sensitivity of radio astronomical stations is often limited by man-made radio emissions due to a variety of activities such as broadcasting operations, radars, and a variety of communication and radiolocation systems. In practical terms, the electromagnetic environment at radio observatories is deteriorating every year. As a result, the performance improvements of the astronomy stations do not always give the expected results because of man-made interference. It may be difficult to attain the sensitivity limits of radio telescopes that are situated even in secluded areas far from human activity.

The vulnerability of radio astronomy stations to *radio frequency interference* (*RFI*) has been described in a number of publications (Pankonin & Price 1981; Waterman 1984; Galt 1990; Maddox 1995; CRAF (Committee on Radio Astronomy Frequencies) 1997; Spoelstra 1997; Kahlmann 1999; Cohen 1999). The received signals of interest are extremely weak: the typical signal-to-noise ratio (*SNR*) is generally −30 dB or less and can be as low as −60 dB. As a consequence of their high sensitivity, radio telescopes are also susceptible to interfering signals from transmitters in adjacent and nearby bands. The influence of *RFI* on a radio astronomy measurement ranges from total disruption by saturation of the receiver to very subtle distortions of the data. While broadband *RFI* raises the general noise level of receivers, thus degrading its sensitivity, any narrow-band *RFI* may imitate spectral lines. For weak interfering signals the degradation of the data may be found only after considerable *off-line* data processing, and may result in false scientific observations.

Radio astronomers are also interested in parts of the radio spectrum that have not been allocated for passive use, because broad-band and narrow-band signals can be found across the whole spectrum. There is a common practice at radio-astronomical stations to monitor the *RFI* environment in those bands and choose observation times and frequency bands so as to receive the minimum possible man-made noise. Investigations of the different types of *RFI* indicate that in some cases it is possible to counteract them actively and avoid contamination of the radio astronomical signals. The combined application of analogue and digital (linear and non-linear) processing can significantly improve the quality of the observational data.

It is important to mention at this time that there is no universal method of RFI mitigation in radio astronomy observations. In particular, the applicability and the success of certain mitigation procedures depend on a number of factors:

1. **The type of radio telescope** – Single dish operations, or connected interferometry, or Very Long Baseline Interferometry. Single dish radio telescopes are especially

Send offprint requests to: P. A. Fridman,
e-mail: fridman@astron.nl

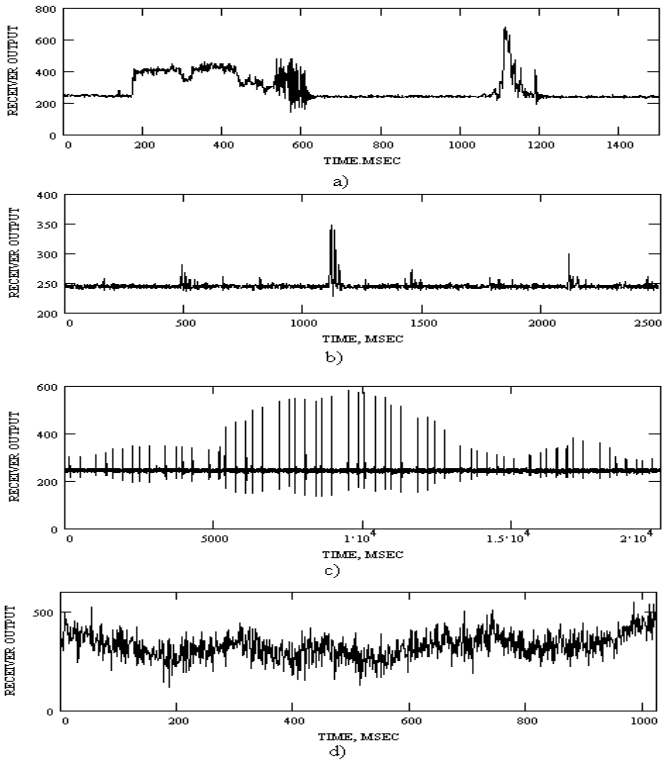

Fig. 1. Examples of *RFI* waveforms in the receiver output versus time: **a)** and **b)** impulse-like *RFI*; **c)** radar impulses; **d)** narrow-band *RFI*.

vulnerable to *RFI* because all incoming *RFI*, entering by scattering or reflection, enters the system coherently. The data obtained with interferometer systems suffer from *RFI* to a lesser degree (Thompson 1982), but any noise power measurements made at each of the antennas for *calibration* purposes will be distorted by the *RFI*.

2. **The type of observations** – Continuum or spectral operations. For continuum observations it is possible to sacrifice some part of the data stream affected by *RFI* and save the remaining part with some loss of observing efficiency. For spectral observations the narrow-band *RFI* and the signal-of-interest can be placed in the same spectral region, such that editing in the spectrum can be done. If they are superposed, it is impossible to delete this particular part of the spectrum.

3. **The type of *RFI*** – Impulse-like bursts, narrow-band or wide-band *RFI*. Theoretical considerations and experimental data show that *RFI* may be represented as a superposition of two types of waveforms: 1) impulse-like bursts and 2) long narrow-band random oscillations (Middleton 1972, 1977; Lemmon 1997). Figure 1 gives examples of the waveforms of various sorts of *RFI*.

2. Methodologies for suppressing *RFI*

The goal of this paper is to consider various mitigation methods and evaluate their applicability and consider how much they may help to decrease the impact of *RFI* on the astronomical data. These methods are all based on the characteristics of modern digital signal processing algorithms and the techniques that are commonly used at existing radio telescopes. Right at the start it should be mentioned that all methods of *RFI* mitigation will be more effective with stronger signals; it becomes increasingly difficult to detect and suppress weaker *RFI* signals.

In evaluating the methodologies for excising or partly suppressing *RFI* in the data, there are three main options:

1. **Rejection in the Temporal Domain.** This type of *RFI* excision is most effective when dealing with strong and short (spiked) bursts of *RFI*. Sampling with sufficiently high frequency and subsequent thresholding may give good results. More complex processing such as the *cumulative sum method* (CUSUM) (Basseville & Nikiforov 1993; Fridman 1996) unites thresholding techniques and adaptive smoothing and provides more flexibility and effectiveness. Weak and long-lasting *RFI* signals are problematic because the threshold methods in the temporal domain do not work in this case. This type of *RFI* might be suppressed by frequency rejection methods, which have limited applicability in spectral line observations.

2. **Frequency rejection.** The whole receiver bandwidth is divided in many channels (using a filterbank or digital correlator techniques) and the channels with *RFI* are suppressed. This type of *RFI* excision can only satisfy observational objectives if there is no special spectral line information in the rejected channels. If the *RFI* signal is concentrated in a few spectral channels, their rejection would not impact strongly on the radiometric sensitivity. If the *RFI* signal in spectral line observations coincides with the spectral window of interest, the *RFI* cannot be simply excised because the signal-of-interest will be also excised. If a time-frequency analysis shows that *RFI* is intermittent (with less than 100% duty cycle), the excision of this *RFI* can be efficient. In general, *adaptive interference cancellation* using an *auxiliary reference antenna* is more effective as a form of spatial filtering.

3. **Spatial filtering.** Spatial filtering methods use the difference in the direction-of-arrival (DOA) of the astronomical signal-of-interest (SOI) and the *RFI*. This type of *adaptive interference cancellation* is similar to the adaptive noise cancellation (ANC) techniques that can be useful for *single dish* observations using an *auxiliary reference antenna pointing off-source*. The *RFI* emission from spatially localized sources could be suppressed using multi-element radio interferometers based on an adaptive array philosophy, where zeros of a synthesized antenna pattern coincide with the DOAs of undesirable signals (adaptive nulling techniques). This approach is being considered for some new-generation radio telescopes (van Ardenne 2000; Bregman 2000). There are some limitations in using this technique for large radio interferometers using sparse antenna arrays with phase-only computer control, which will result in a complex impact on the imaging process. One of the possible applications for this technique could be a tied-array (phased-array) mode, where only one output (two polarizations X, Y or R, L) is produced for use in VLBI or pulsar observations.

Spatial filtering is effective when the *RFI* is strongly correlated at the individual antennas of the radio telescope, which may be the case for common radar and communications half-wavelength phased-arrays.

Single dish radio telescopes with large antennas employ total power receivers as their output, which is particularly susceptible to *RFI*, because it is 100% correlated at the antenna feed. Therefore, the *RFI* power is fully added to the system and to the desired radio source noise power. Even very weak *RFI* will be dangerous after long averaging by mimicking wanted astronomical signals.

RFI at the sites of VLBI system separated by hundreds and thousands of kilometers, are practically uncorrelated. The impact of *RFI* at the correlator output is an increased variance. This change in the variance will be significant when the *RFI* power becomes comparable with the system noise power.

Connected interferometers form an intermediate type of radio telescope. For these systems the *RFI* at nearby adjacent antennas (with less than 100 m separation) is highly correlated, but it becomes less correlated at larger separations (baselines) of 1 km and especially at baselines from 10–100 km. Because of non-continuous spacings, the effectiveness of the adaptive nulling technique cannot be as high as that of the continuous-like half-wavelength phased arrays.

2.1. Parameters describing the results of the methods

When evaluating a certain *RFI* mitigation method, the following two questions need to be asked:

a. What is the level of suppression of the *RFI* signal?

b. What is the loss of the signal-of-interest as a result of the *RFI* mitigation also including the total amount of data loss?

The general parameters that describe the method and quantify the results of *RFI* suppression are the following:

1. The intensity of the *RFI* is characterized by the input ratio of the system-noise variance to the *RFI* variance:

$$Q_1 = \frac{\sigma^2_{\rm SYS}}{\sigma^2_{RFI}}. \tag{1}$$

2. The bandwidth occupied by an *RFI* signal is characterized by the ratio of signal-of-interest (or receiver) bandwidth to the *RFI* bandwidth:

$$Q_2 = \frac{\Delta f_{\rm rec}}{\Delta F_{RFI}}. \tag{2}$$

3. The processing gain obtained after *RFI* suppression is characterized by the ratio:

$$G_{\rm proc} = \frac{SNR(\text{after processing})}{SNR(\text{before processing})}. \tag{3}$$

4. The loss arising from the *RFI* suppression relative to the ideal situation (no *RFI*) is:

$$R_{\rm prc} = \frac{SNR(\text{after processing})}{SNR(\text{without } RFI)}, \tag{4}$$

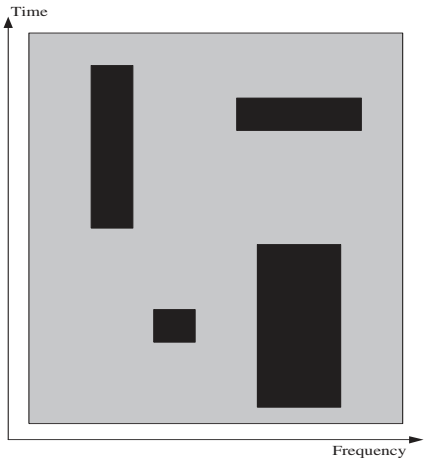

Fig. 2. Time-frequency plane of telescope data. The grey areas represent the system noise, and the black areas represent data with *RFI*.

where Δf is the receiver bandwidth, Δf_{RFI} is the bandwidth occupied by the *RFI*, $\sigma^2_{\rm SYS}$ is the system-noise variance, and σ^2_{RFI} is the *RFI* variance. The signal-to-noise ratio (SNR) is determined as the ratio of the radio telescope output resulting from the SOI to the rms of the fluctuations at this output.

3. Five methods of *RFI* suppression

In this section a number of *RFI* suppression methods will be considered. An evaluation of the processing gain and loss parameters for each of these methods can be found in the corresponding section in the Appendix (Sect. 6).

3.1. Excision in the time-frequency domain – thresholding

A general description of a telescope input signal $x(t)$ is

$$x(t) = x_{\rm sig}(t) + x_{\rm sys}(t) + x_{RFI}(t), \tag{5}$$

where $x_{\rm sig}(t)$ is the signal-of-interest, $x_{\rm sys}(t)$ is the total system-noise (the radio sky plus the feed plus the receiver), and $x_{RFI}(t)$ is the *RFI* signal. $x_{\rm sig}(t)$ and $x_{\rm sys}(t)$ are noise-like signals with a Gaussian probability distribution, zero mean, and with variances $\sigma^2_{\rm sig}$ and $\sigma^2_{\rm sys}$, respectively. $x_{RFI}(t)$ is a signal waveform whose statistical characteristics, probability distribution and moments can be highly variable due to the intrinsic properties of an *RFI* source. This variability is caused by motion of the source, the movement of the tracking radio antenna, the change of the signal content of broadcasting or mobile transmissions, and constructive or destructive interference due to multi-path propagation, etc.

The signals received by a radio telescope can be represented in a simplified form in the time-frequency $(t - F)$ plane (Fig. 2), where the grey parts are the areas free from *RFI* with only the presence of $x_{\rm sig}(t) + x_{\rm sys}(t)$, and where the black parts correspond to the presence of *RFI*. Thus a

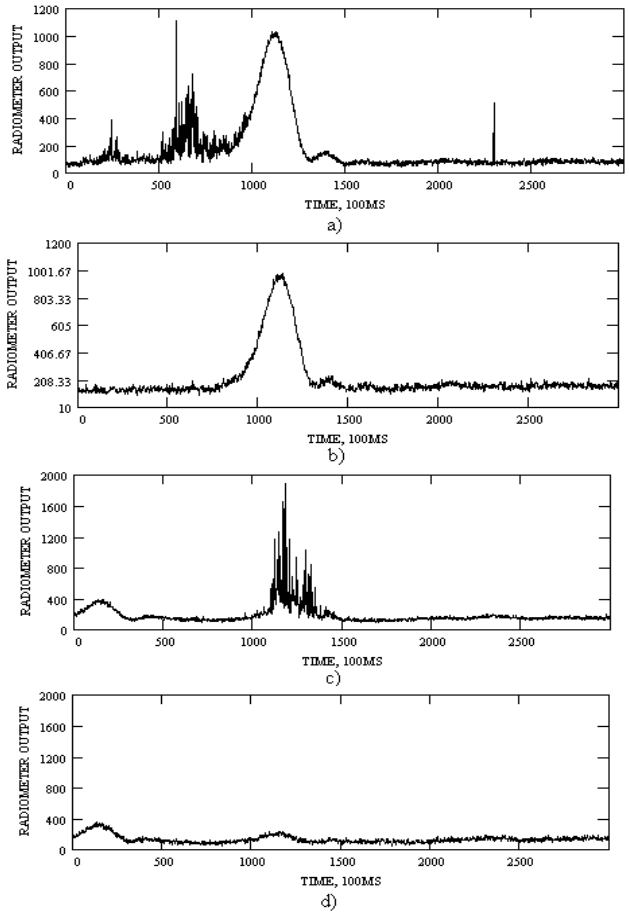

Fig. 3. Source scans made at the RATAN-600 at $\lambda 31$ cm using *RFI* excision in the temporal domain: **a)** without *RFI* excision, **b)** with *RFI* excision, both records were made simultaneously; **c)** and **d)** give the same sequence for another radio source.

time-frequency analysis of $x(t)$ with sufficiently high resolution in both axes must be performed in order to detect these "black" zones and excise them.

It is difficult to prescribe a time resolution δt and a frequency resolution δf for detection of all possible varieties of *RFI*. However, some recommendations can be made for the range of these values: $\delta t \approx 0.1{-}1$ μs and of $\delta f \approx 1{-}50$ kHz. Especially this last number is conditional and depends on the receiver bandwidth $\Delta f_{\rm rec}$, which may vary from dozens of kHz to hundreds of MHz. When the ratio of excised data to the total amount of data $\Delta f \cdot T$ is less than 5–10%, where T is the integration time, this method of *RFI* mitigation can be used well for continuum observations. The quantitative estimates for the gain and loss are given in the Appendix.

Figure 3 illustrates some *RFI* mitigation results in the temporal domain during observations with the RATAN-600 telescope (Fridman & Berlin 1996). The procedure uses post-detection sampling with a time resolution of 4 μs and an *RFI* detection and excision method by *thresholding* at the $\pm 3\sigma_{\rm sys}$ level. Subsequent time averaging to obtain the necessary SNR gain $\sim\sqrt{\Delta f \cdot T}$ provides additional suppression of impulse-like *RFI*.

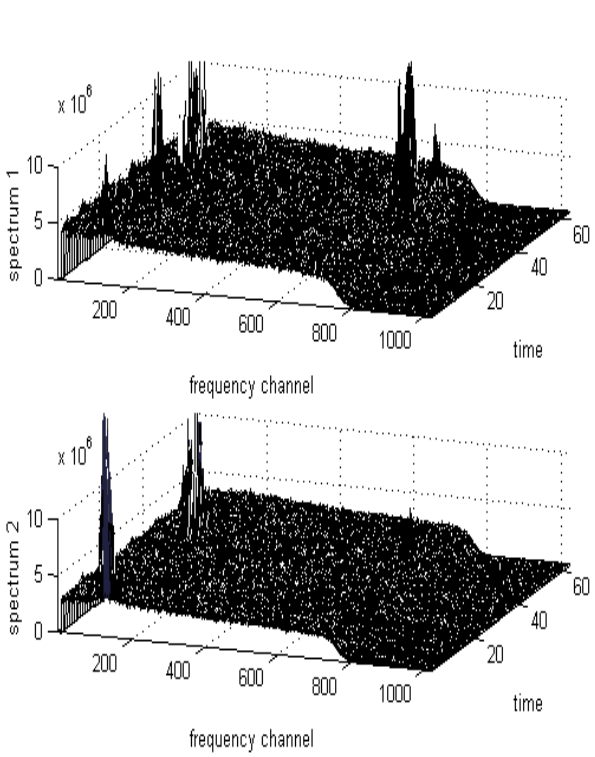

Fig. 4. The time evolution of the autocorrelation (power) spectra affected by *RFI* taken with the WSRT at 6 cm receiver with bandwidth $\Delta f = 10$ MHz and a sampling speed of $f_{\rm sample} = 12.5$ MS/s: **a)** the signal at telescope RT1, **b)** the signal at telescope RT2.

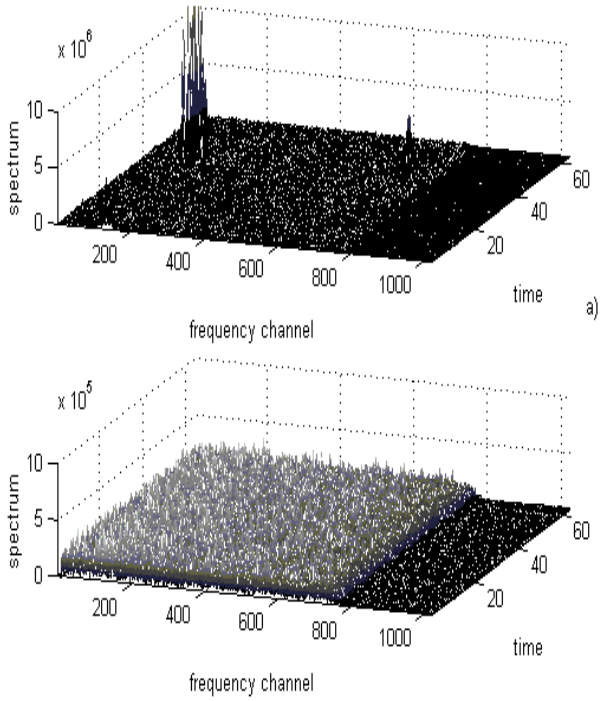

Fig. 5. The time evolution of the cross-spectrum magnitudes for the data in Fig. 4: **a)** the dirty data without *RFI* excision, **b)** the cleaned data after *RFI* excision.

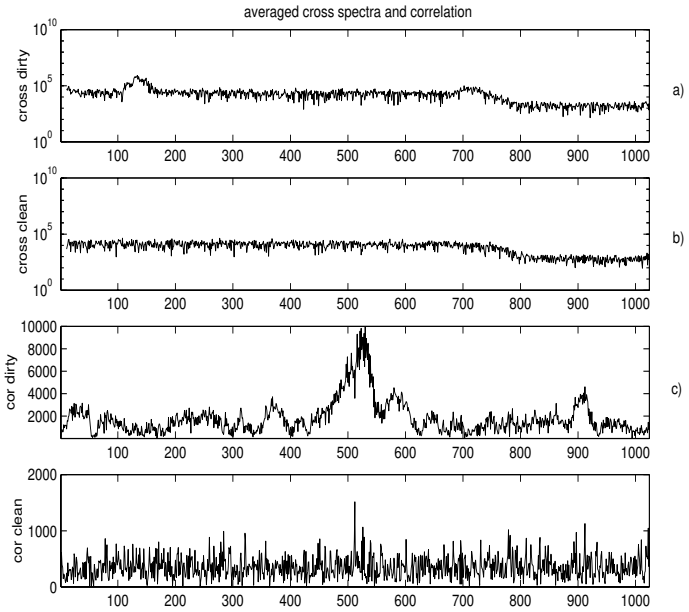

Fig. 6. The averaged cross-correlation spectra corresponding to Figs. 4 and 5 are given on a logarithmic scale in the upper frames: **a)** no *RFI* excision applied; **b)** with *RFI* excision applied. The averaged cross-correlation functions are given in the bottom frames: **c)** no *RFI* excision applied; **d)** with *RFI* excision applied.

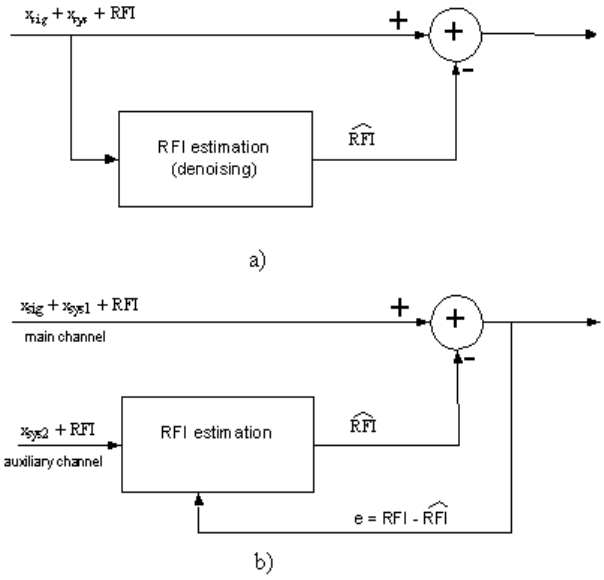

Fig. 7. Methods of *RFI* cancellation using *autoclean filtering* as described in Sect. 3.2 (frame **a)** and *RFI excision by filtering* using a reference channel as described in Sect. 3.3 (frame **b)**).

Figures 4–6 give examples of *RFI* excision in the frequency-domain at the Westerbork Synthesis Radio Telescope (WSRT). The data were recorded during a VLBI session at the WSRT at 6 cm on 8 June 2000. The baseband outputs of two radio telescopes (RT1 and RT2) were digitized and their power spectra were calculated with the help of a DSP processing unit (TMS320C6201, *Signatec* PMP-8 board). Figures 4a and 4b represent the autocorrelation spectra including *RFI*. The cross-correlation spectrum of this raw data is represented in Fig. 5a, while the *cleaned* cross-spectrum after *RFI* excision is shown in Fig. 5b. The time-averages of the cross-correlation spectra of Fig. 5 are given on a logarithmic scale in Figs. 6a,b. The time-averaged dirty and clean cross-correlation functions (magnitudes) are shown in Figs. 6c,d. The five-fold difference in the magnitude in Fig. 6c shows that a large false correlation occurs in the presence of *RFI*. The peak in the cross-correlation function in Fig. 6d corresponds to a weak (but real) radio source. Blanking in the time-domain can be very effective when the *RFI* detection is done after a statistical analysis of the correlator lag outputs, such that the blanking of the correlator output is triggered by the detection of *RFI* (Weber et al. 1997).

3.2. Excision using filtering techniques

Temporally spread and strongly correlated *RFI* (see Fig. 1d) can be suppressed using cancellation techniques based on estimating the *RFI* waveform and subsequently subtracting it from the *signal+RFI* mixture:

$$x_{\mathrm{CLEAN}}(t) = x(t) - \widehat{x}_{RFI}(t). \tag{6}$$

The *RFI* waveform (or its complex spectrum) $\widehat{x}_{RFI}(t)$ can be estimated using any available filtering technique (spline-smoothing, Wiener filtering, wavelet denoising, parametric identification, etc.). The estimate can then be subtracted from the input data in the temporal or frequency domain. The principle of this *autoclean method* in the time and frequency domain is shown in the diagram of Fig. 7a.

The following example uses WSRT data to describe the use of this *autoclean method* in the frequency domain. Figures 8a,b display the time evolution of the power spectra at two adjacent WSRT antennas at $\lambda = 49$ cm. Figures 9a,b show the averaged power spectra corresponding to Fig. 8. The complex instantaneous spectra at each of the two antennas were processed using this "*RFI* estimation – subtraction" technique. Figure 9d shows the "dirty" cross-correlation function (without *RFI* suppression), while Fig. 9c shows the "cleaned" cross-correlation function (after *RFI* suppression).

One necessary comment should be made about using these *thresholding* (Sect. 3.1) and *autoclean* (this section) methods: the basic form of the system noise spectrum must be known beforehand. Because it is not ideally rectangular, it repeats the form of the receiver transfer function. These algorithms depend on the "quiet", undisturbed baseband spectrum as a reference in order to compare it with the running spectra with *RFI*.

An example of a *parametric approach* to this type of *RFI* cancellation can be found in Ellingson et al. (2000). In this paper the strong interfering signal of a GLONASS satellite is represented by a parametric model, such that

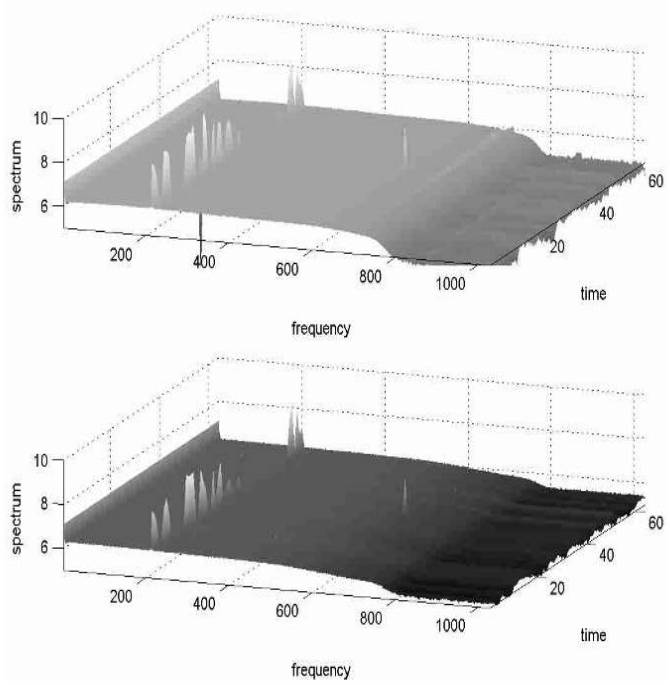

Fig. 8. An example of the time evolution of power spectra with *RFI* on a logarithmic scale. The bandwidth is $\Delta f = 10$ MHz and the sampling frequency is $f_{\rm sample} = 25$ MHz. The data from **a)** RT1 and **b)** RT2 are the basis for the discussions in Sect. 3.2 and the excising results in Fig. 9.

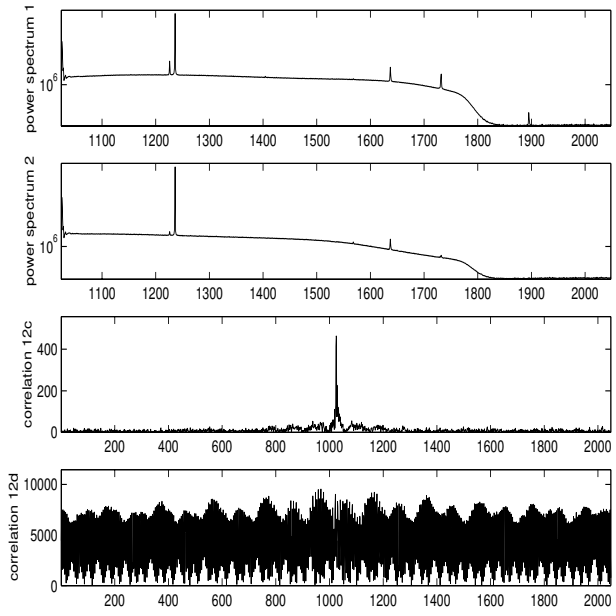

Fig. 9. Excision by autoclean filtering of the data given in Fig. 8: **a)** the averaged power spectrum of RT1, **b)** the averaged power spectrum of RT2, **c)** the cross-correlation function after the *RFI* suppression, and **d)** the cross-correlation function with *RFI* present.

its parameters – Doppler frequency, phase code, and complex amplitude – were calculated for each separate data block. The parametric model of the *RFI* was then used to calculate an *RFI* waveform, which was subsequently subtracted from the *RFI + noise signal* mixture. The signal-of-interest, in this case an OH spectral line at 1612 MHz, was not significantly distorted during the *RFI* suppression process.

3.3. Adaptive interference cancellation using reference channels

A separate, dedicated reference channel may be used in order to obtain an independent estimate of the *RFI* signal $\widehat{x}_{\rm RFI}(t)$. This technique has been used for a long time in digital signal processing and is called *adaptive noise cancelling* (ANC) (Widrow & Stearnes 1985). Figure 7b shows a block diagram relating to the application of this type of algorithm. There are two data channels: a main channel with the radio telescope pointing *on source and containing the RFI signal*, and an auxiliary or reference channel at a separate antenna pointing *off source and also containing the RFI signal*. While both channels contain the *RFI* signal, they are not identical due to the different propagation paths and radio receivers. To the procedure now calls for adjusting the *RFI* signal in the reference channel with the help of an adaptive filter, such that the error signal $e = x_{\rm main} - x_{\rm ref} \longrightarrow 0$. The value of this error signal is used for adjusting the filter.

This procedure can be applied both in the temporal domain (*adaptive filtering*) and in the frequency domain using an $FFT \rightarrow$ *adaptation in each frequency bin* $\rightarrow FFT^{-1}$) procedure. This kind of *RFI* cancellation is especially useful for spectral line observations, where the *RFI* and the signal-of-interest occupy the same frequency domain.

Figures 10 and 11 illustrate the results of using the ANC procedure with WSRT data at 428 MHz. Figures 10a,b shows the power spectra at the outputs of the main and the reference channels. Figure 11 shows the *cleaned* power spectrum of the main channel.

Other examples of the use of a reference channel can be found in Barnbaum & Bradley (1998) and Briggs et al. (2000). The second paper also discusses *post-detection RFI* suppression. In these papers the complex spectrum of the *RFI* estimate was obtained with the help of closure relations using *four* averaged correlator output signals all containing *RFI*: two polarizations for the main channel and two polarizations for the reference channel. Subsequently the power spectrum estimate of the *RFI* was subtracted from the power spectrum of the main channel. This method is particularly effective for multi-feed single dish radio telescopes.

3.4. Spatial filtering with multi-element systems

Adaptive-nulling of a synthesized pattern in the direction of *RFI* sources has been widely used in radar and communication systems (*smart antennas*). This technique

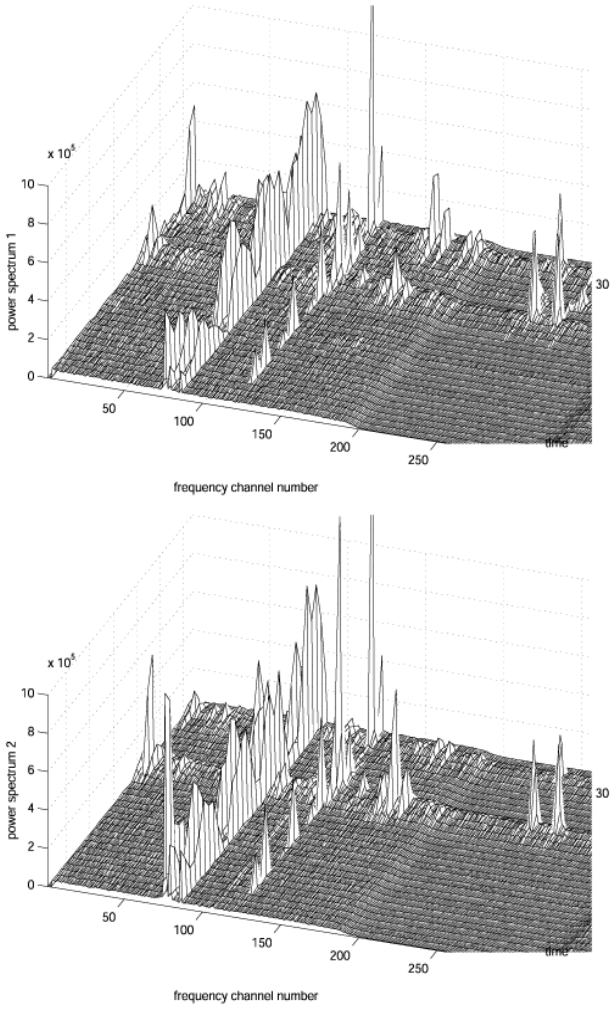

Fig. 10. The time evolution of the power spectrum of the main channel of RT1 is given in frame a and of the reference channel of RT2 in frame b. This data is used to obtain the effectiveness of *adaptive noise cancellation* using a reference channel as given in Fig. 11.

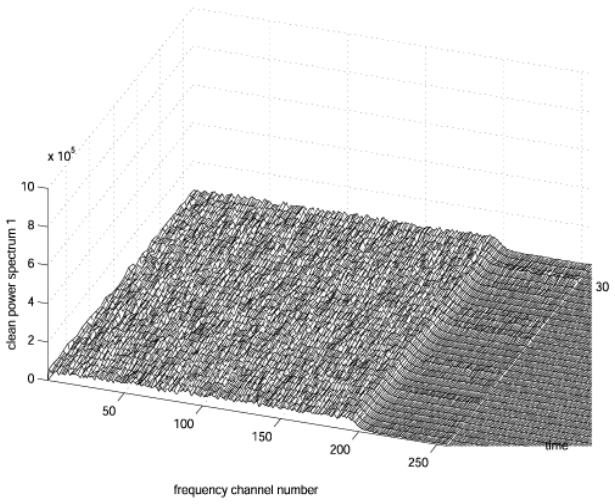

Fig. 11. The time evolution of the "clean" power spectrum of the main channel RT1 after applying an *adaptive noise cancellation* technique with a reference channel.

can be applied in multi-element radio interferometers (MERIs) but has the following limitations:

1. Radio astronomy MERIs are generally very sparse arrays. The distances between antennas are equal to hundreds and thousands of meters, which is significantly larger than the $\lambda/2$ separation of ordinary phased-arrays. Therefore, adaptive-nulling is particularly effective for narrow-channel processing (at the kHz level).

2. Radio astronomy MERIs are correlation arrays and are not additive. The antenna pattern is not synthesized in real-time but rather *off-line* after several (up to 12) hours of tracking the radio source. In principle, it is possible to introduce complex weighting during the image processing stage and do the RFI suppression off-line. But this also means that time averaging during correlation requires the use of small time intervals and narrow bands, so as not to smooth the RFI in frequency and time. This type of processing requires a significant increase of computational power and also requires changes in the image-making software. Several aspects of this problem have been discussed in Leshem et al. (2000).

3. All spatial adaptive-nulling procedures presume that the RFI sources are well localized in space, which is not always the case.

In this section, we discuss some test WSRT observations using a spatial filtering technique based on adaptive complex weighting of the data. The signals from two antennas RT1 and RT2 (Fig. 12) were Fourier transformed and their complex spectra were combined at each frequency bin in order to get an estimate of the RFI. These RFI estimates were then subtracted from each of the RT1 and RT2 signals. The RFI estimates were made, while minimizing the error signals at the subtracted outputs. Subsequently the cross-correlation functions and the corresponding cross-spectra were calculated. Figure 13 shows the results of test observations of 3C 48 at $\lambda = 49$ cm with a sampling frequency of $\Delta f_{\rm s} = 10$ MHz. Figures 13c,d show the *cleaned* spectrum after RFI subtraction, and the *dirty* spectrum without RFI suppression.

Real-time adaptive-nulling techniques are particularly suitable for the future generation of radio telescopes using phased-array techniques (van Ardenne et al. 2000; Bregman 2000). It is also possible to apply adaptive-nulling in existing MERIs operating in a so-called tied-array mode, for example, during VLBI operations or pulsar observations (see Moran 1995). Currently operating MERIs are severely limited because they have computer control only of the antenna phases but not of their amplitudes. This situation can be optimised by introducing small *phase-only* perturbations in order to minimize the total-power output of a tied-array that contains a strong narrow-band RFI signal and a weak signal-of-interest. Such phase perturbations should be calculated, while optimising the gain of the synthesized antenna main lobe at the SOI direction. This typical optimisation problem can be executed with any algorithm, that is robust enough to deal with the multi-modality of the optimization function.

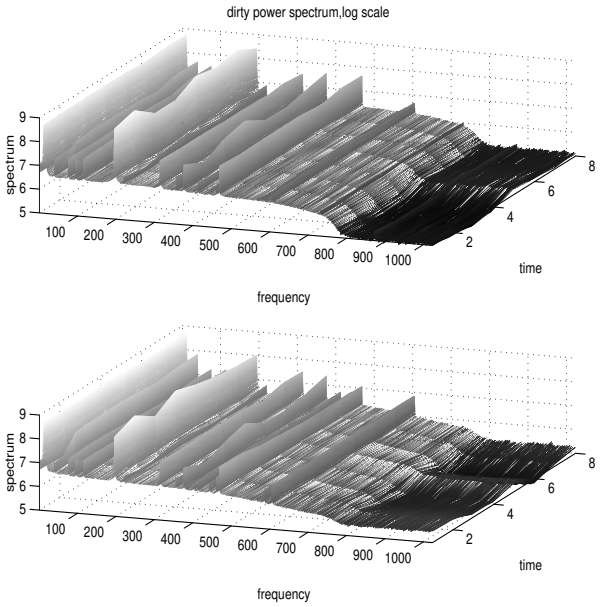

Fig. 12. The time evolution of power spectra for two antennas **a)** RT1, **b)** RT2. The wavelength of the data is $\lambda = 49$ cm and the bandwidth $\Delta f = 10$ MHz. This data for source 3C 48 will be used to demonstrate the spatial filtering procedure, which is displayed in Fig. 13.

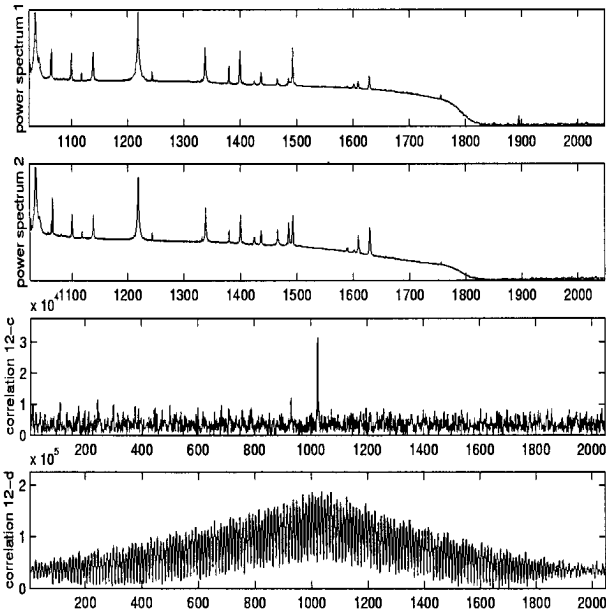

Fig. 13. The averaged power spectra for antennas RT1 and RT2 is given in **a)** and **b)** corresponding to the data in Fig. 12. The complex cross-correlation function between RT1 and RT2 is given (in magnitudes) in **c)** the cleaned spectrum, and in **d)** the dirty spectrum ($\lambda = 49$ cm, $\Delta f = 10$ MHz, source 3C 48).

An example of such an application using a *genetic algorithm* for solving the optimisation problem is represented in Figs. 14–16. Figure 14 shows the calculated unmodified (solid line) and adapted (dashed line) beam patterns of a linear MERI with 14 antenna at separations of 144m and at a central frequency of $f_0 = 1420$ MHz. The direction of arrival (DOA) of the signal of interest (SOI) is at 0°

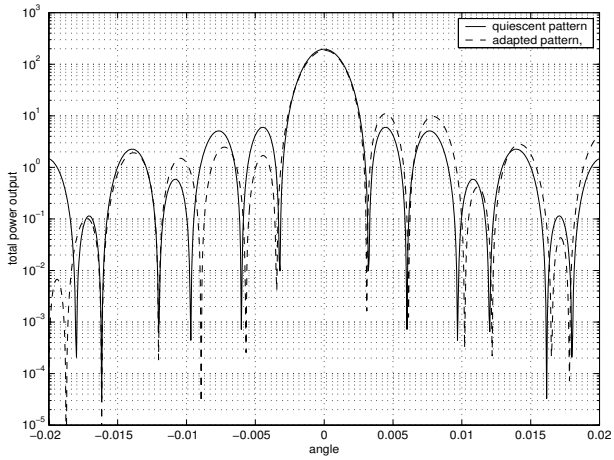

Fig. 14. The unmodified (solid line) and the phase-only adapted (dashed line) main-beam pattern for a 14 element array with 144 m spacings at a central frequency of 1420 MHz.

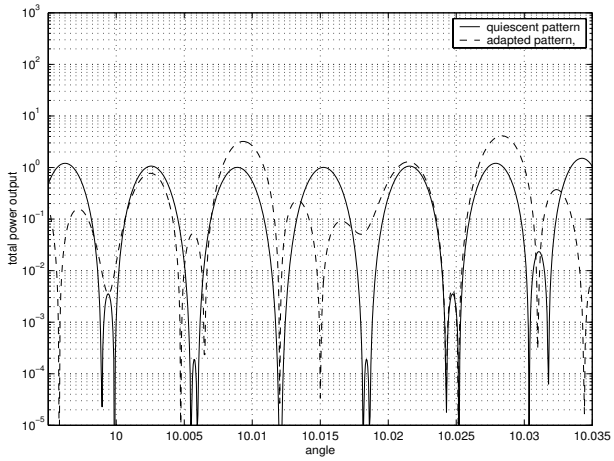

Fig. 15. The unmodified (solid line) and the phase-only adapted (dashed line) beam pattern of the 14 element array in Fig. 14 in the direction of the *RFI* source at +10.015°.

and the DOA of two sources of *RFI* are at +10.015° and −20.1°, respectively. Figures 15 and 16 show fragments of the beam patterns in the two directions of the *RFI*, which were purposely chosen to coincide with the maxima of the unmodified side lobes. The distribution of the phase corrections corresponding to this adapted pattern is given in Fig. 17.

3.5. Excision based on a probability distribution analysis of the power spectrum

The method of *RFI* excision based on a *probability distribution analysis* of the output signal of the radio telescope has applications for both spectral line and continuum observations (Fridman 2001). The signals of the system noise and the radio source generally have a Gaussian distribution with a zero mean. Fourier transformation of such an ideal signal also gives real and imaginary components in every spectral bin, that are Gaussian random values with zero means. On the other hand, the instantaneous power spectrum (the square of magnitude of the complex

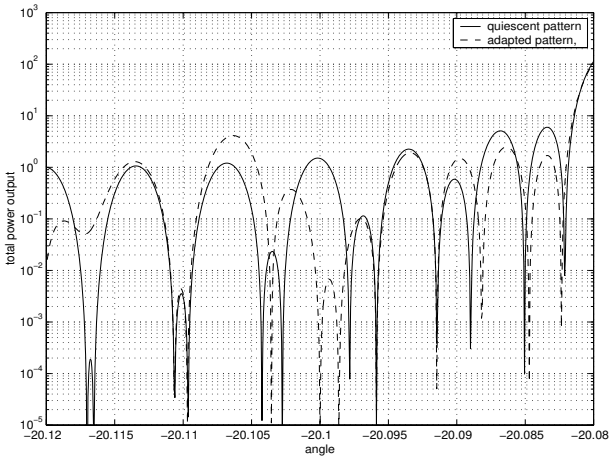

Fig. 16. The unmodified (solid line) and the phase-only adapted (dashed line) beam pattern of the 14 element array in Fig. 14 in the direction of the *RFI* source at −20.1°.

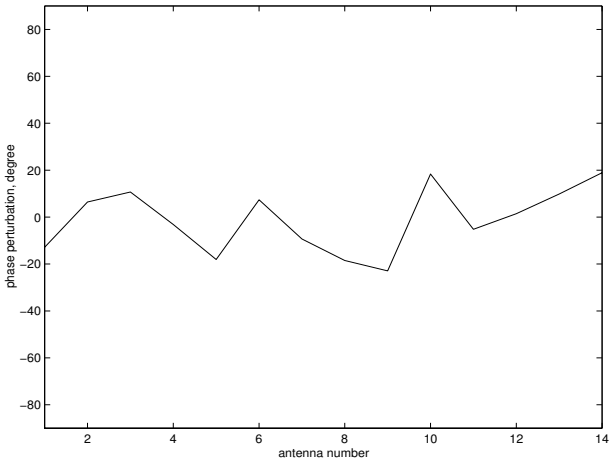

Fig. 17. The distribution of the phase corrections at the 14 antennas corresponding to the adapted beam patterns described in Figs. 14–16.

spectrum) has an exponential distribution, which can be described as a chi-squared distribution with two degrees of freedom.

The presence of an *RFI* signal modifies the ideal input signal further and yields a change of its statistics. The modified power spectrum will now have a *non-central chi-squared distribution with two degrees of freedom*. Standard radio astronomy practices employ significant averaging of the power spectrum, which would again convert the probability distribution of the averaged power spectrum into a Gaussian distribution. Therefore, only real-time analysis by means of DSP processing of the distribution *before averaging* will allow a separation of the two signal components.

Test observations at the WSRT have been used to demonstrate the effectiveness of this digital spectral analysis. The baseband (0–1.25 MHz) signal at the analogue output of the WSRT-DLB subsystem for one of the antennas (RT6) has been digitized in a 12-bit analogue to digital converter and then supplied to a *Signatec* PMP-8 system,

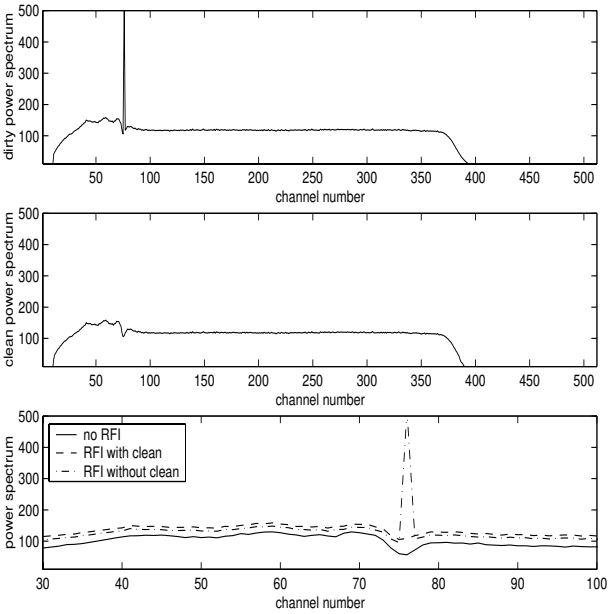

Fig. 18. *RFI* excision based on a probability analysis of the signal. The WSRT data were taken with bandwidth = 1.25 MHz, half-sampling frequency = 1.563 MHz, and frequency resolution = 3.052 kHz. **a)** A total power spectrum of a galactic HI emission spectrum and an absorption line towards the Crab Nebula at 1420.4 MHz with an artificial *RFI* signal at 1420.397 MHz; **b)** The same data after *RFI* excision made simultaneously; **c)** The spectral window around the spectral line (channels 30–100) with superposed spectra from **a)** and **b)** and a spectrum without any *RFI*.

where the *FFT* and the averaged statistical parameters are calculated.

Figure 18 shows the results of these test observations of the 21 cm HI line in the direction of the Crab Nebula. Since no transmissions are allowed in the 1400–1427 MHz band, an artificial CW *RFI* signal was transmitted in the direction of the RT6 antenna from the WSRT control building. The power spectra of Fig. 18 show the non-processed data and the processed data generated simultaneously. The clear *RFI* signal in the non-processed data is suppressed by about 17 dB in the processed spectrum.

This method can be used both for spectral line and continuum observations. In the continuum case, parts of the spectrum with a "non-Gaussian signature" may be blanked or filtered out. However, it should be mentioned that reliable estimates of the higher moments of the data (or cumulants) will require more averaging than for the first moment (the mean). This is important for mitigation of the weak *RFI*. Large averaging intervals will smooth the variability of the *RFI* and will yield estimates with a considerable bias. Therefore, a trade-off should be adopted, which implies some limitations on the detection and limited excision of weak *RFI* signals. This principle applies equally to other *RFI* mitigation methods: stronger *RFI* signals can be easier detected and suppressed.

4. An evaluation of the methods

In this section we consider the effectiveness and applicability of the various *RFI* mitigation methods for different types of telescopes and telescope operations. There are three principal stages in the astronomical data-taking process at which mitigation methods can be used:

1. *Real-time pre-detection and pre-correlation baseband processing* is based on time-frequency analysis and adaptive noise cancellation using reference channels. This approach requires the implementation of fast digital processing techniques (>100 GIPs), which can already be achieved with modern digital signal processing hardware based on DSP and FPGA devices. However, the implementation of these *RFI* mitigation techniques may not be easy and may sometimes be technically impossible in the existing backends.

2. *Real-time post-correlation processing* techniques may introduce time-frequency analysis as part of the correlation process and before data averaging. The implementation of these methods will also require special hardware as part of the existing backends.

3. *Off-line* post-detection and post-correlation processing techniques, such as adaptive-nulling and those using closure relations and reference signals, may capitalize on the differences in the spatial signatures of the signal-of-interest and the *RFI* signal. This approach is attractive from a practical point, because it requires no change in the radio telescope backend hardware. However, these methods may be less effective than real-time processing.

It should be mentioned here that applications of these methods do not exclude other technical measures, such as the development of front-ends with high linearity and of analogue filters with low insertion (<0.05 dB) losses and high stop-band attenuation (>70 dB).

4.1. Single dish telescopes

Single dish telescopes are most susceptible to *RFI* signals. Depending on the type of observations and on the available electronics, the following methods may be considered for application:

1. Continuum observations are best served with post-detector blanking and filtering with high temporal (at least microseconds) and frequency (less than 1 kHz) resolution.

2. Spectral observations are best served with methods using a reference antenna (or reference feed). In this case an estimate of the *RFI* signal may be subtracted from the input signal with real-time adaptive filter processing, or with off-line processing using the complex closure-amplitudes of the correlated data.

Analysis of the higher-order statistics of the received signals is an effective method of *RFI* detection and mitigation, but it requires some considerable modifications in the existing spectrometers, which measure only the mean of the spectra. New generations of radio astronomy spectrometers should also determine the higher moments of the spectrum. Using the polyspectra analysis may also be useful for radio interferometers experiencing strong (atmospheric) phase errors.

4.2. Large connected radio interferometers

Interferometers such as the WSRT, VLA, GMRT, and MERLIN, are less vulnerable with respect to man-made *RFI*. Modulation of the *RFI* by routine fringe-stopping and decorrelation by delay compensation procedures constitute a natural suppression of weak *RFI* signals in interferometers. Strong *RFI* signals cause a significant change of the noise-variance before correlation and hence they distort the complex visibilities of the correlator output. Thus pre-correlation real-time blanking and filtering with and without a reference antenna can result in a considerable gain in *RFI* suppression.

RFI suppression using post-correlation complex weighting (adaptive nulling) may be also effective for interferometers as in the case of ordinary half-wavelength phased-arrays, but it will change the amplitude-phase structure of image visibilities. Therefore continuous "book-keeping" of these weights is necessary, in order to take them into account at a later time during the image synthesis stages of CLEAN + self-calibration procedures.

Spatial filtering is effective only if the *RFI* is significantly correlated at the radio interferometer antenna sites. This is likely not to be the case generally, because of multipath propagation effects and other limitations due to the base – radio source – *RFI* source geometry. The use of a special reference antenna pointing at the *RFI* source is particularly attractive when subsequent post-correlation processing is used based on complex amplitude-closure relations. This procedure does not interfere with the existing radio telescope infrastructure and gives a high signal-to-noise ratio with respect to the *RFI*.

4.3. Very long baseline interferometry

VLBI observations are most robust to *RFI* due to the very large baselines, because the *RFI* signals are practically uncorrelated at the different stations. The calibration data at each site is also susceptible to *RFI*, such as is the case for single dish observations. Therefore, *RFI* blanking at each of the VLBI sites may be considered as desirable for the new generation of VLBI video converters (Mark-V).

4.4. An evaluation

A quantitative evaluation of the effectiveness of the different methods is not always possible. In the first place, the *RFI* mitigation algorithms are often non-linear procedures. Secondly, the suppression of an *RFI* signal achieved with a certain method depends on the fractional intensity of the *RFI* signal (i.e. the INR) and its spatial, temporal and spectral characteristics. The extreme example is the simplest method of thresholding in the temporal or

frequency domains. If we assume that the *RFI* signal is 100 dB(!) higher than the system noise and we ignore the non-linearities in the receiver, this "100 dB" *RFI* can easily be detected and excised. As a result we have a suppression gain of $\gg$100 dB, because there is no *RFI* left over at all. However, there will be a certain growth of the noise standard deviation at the correlator or detector output due to a deletion of a number of data samples. The effect will thus be visible as a loss in the *SNR*.

Therefore, a simplified approach in the evaluation of the effectiveness of the *RFI* mitigation method is affected by its dependence on the particulars of the *RFI* situation. The estimates in the Appendix provide the approximate bounds for the gain and loss. A practical limit for each method depends on the INR. Sometimes it is not possible to remove the *RFI* below the noise level of the data. This is also useful for understanding the cumulative effect of *RFI* mitigation at various stages of the data acquisition process, where different methods may be applied simultaneously, such as filters in the frontend, real-time processing, post-correlation processing, etc. The *RFI* characteristics change after each stage of *RFI* suppression. The total *RFI* is thus not the linear sum of what is maximally possible at each stage but rather a sum of what is practically possible considering the parameters of the *RFI* signal encountered.

4.5. An RFI database

An *RFI* database should be created at each radio telescope in order to provide guidance for observational procedures and for choosing appropriate *RFI* mitigation methods. The combination of a database and hardware/software facilities forms the basis for an *RFI* mitigation system and should be used at terrestrial radio telescopes operating in hostile electro-magnetic environments.

5. Conclusions

1. While there are different types of radio telescopes, different observational procedures and different types of *RFI* signals,*there is no universal method of RFI mitigation.*
2. A choice of the proper *RFI* mitigation method should be made taking into account the particulars of the *RFI* environment of each site.
3. The application of digital *RFI* mitigation techniques in radio astronomy is still at the beginning of its development. However, there are encouraging results with theoretical and computer simulations, and with *on-line* and *off-line* data processing.
4. Existing single-dish telescopes and multi-element radio interferometers should be equipped with *RFI* mitigation facilities in order to fully realize their observational potential.
5. The next generation radio telescopes should be designed from the outset with *RFI* mitigation facilities in place.
6. There are a number of points in the astronomical data-taking process where *RFI* mitigation methods may be applied. Pre-processing occurs between the detectors and the correlator. Real-time processing may utilize the processing capability of the correlator in order to reduce the effects of the *RFI*. Post-processing techniques may use excising techniques or the data from reference antennas.

6. Appendix

Estimates of the gain, which is the degree of *RFI* suppression, and the loss, which is the degradation of the signal-of-interest after processing, are presented in this section for different methods of *RFI* mitigation.

6.1. Excision in the time-frequency domain

Let us consider the time-frequency $t \bigoplus f$-plane of Figure 2, where grey areas correspond to a system noise (no *RFI*) and black areas indicate the presence of *RFI*. The total number of data points in the $t \bigoplus f$-plane is M. A fraction $\beta = S_{RFI}/S_{\rm tot}$ is occupied by *RFI*, where S_{RFI} is the total area occupied by *RFI*, and $S_{\rm tot}$ is the total area of the $t \bigoplus f$-plane. The $t \bigoplus f$-plane is used for data averaging to get a gain $\sim\sqrt{M}$ in the signal-to-system noise ratio after correlation (or total power detector, TPD). β is naturally less than one, $0 \leq \beta < 1$, because otherwise the excision process will also excise the signal-of-interest.

Let us first consider the idealized situation: all *RFI* are 100% detected and excised. What are the benefits in terms of gain and loss as defined by formulas 3 and 4? Let $\mathcal{P}_{\rm sig}, \mathcal{P}_{\rm sys}$, and $\mathcal{P}_{RFI}$ be the antenna signal, the system noise, and the *RFI* spectral power densities, respectively, with $\alpha = \mathcal{P}_{RFI}/\mathcal{P}_{\rm sys}$. The rms of the fluctuations at the output of the correlator (or the TPD) in the absence of *RFI* is $\mathcal{P}_{\rm sig} \ll \mathcal{P}_{\rm sys}$ $\mathrm{rms}_0 = \frac{\mathcal{P}_{\rm sys}}{\sqrt{M}}$. The signal-to-noise ratio (*SNR*) in the absence of *RFI* is $SNR_0 = \frac{\mathcal{P}_{\rm sig}}{\mathrm{rms}_0} = \frac{\mathcal{P}_{\rm sig}}{\mathcal{P}_{\rm sys}}\sqrt{M}$.

The rms and the *SNR* in the presence of *RFI* is expressed as

$\mathrm{rms}_{RFI} = \sqrt{(\frac{\mathcal{P}_{\rm sys}}{\sqrt{M}})^2 + \beta(\mathcal{P}_{RFI})^2} = \mathcal{P}_{\rm sys}\sqrt{\frac{1}{M} + \beta\alpha^2}$

and $SNR_{RFI} = (\mathcal{P}_{\rm sig}/\mathcal{P}_{\rm sys})\frac{1}{\sqrt{\frac{1}{M}+\beta\alpha^2}}$.

At this point we assume that the *RFI* is not reduced after M averaging , such that the *RFI* is 100% correlated, $\mathrm{rms}_{\rm EXC} = \frac{\mathcal{P}_{\rm sys}}{\sqrt{M(1-\beta)}}$,

and $SNR_{\rm EXC} = (\mathcal{P}_{\rm sig}/\mathcal{P}_{\rm sys})\sqrt{M(1-\beta)}$.

The evaluation parameters are as follows: the gain due to *RFI* suppression and the *SNR* loss are

$G_{\rm EXC} = \frac{SNR_{\rm EXC}}{SNR_{RFI}} = \sqrt{\frac{1}{M} + \beta\alpha^2}\sqrt{M(1-\beta)}$,

and $R_{\rm EXC} = \frac{SNR_{\rm EXC}}{SNR_0} = \sqrt{(1-\beta)}$. This approach presumes that the *RFI* is 100% correlated at the different locations of the radio interferometer and that the rms_{RFI} reflects the harmful effect of the *RFI* signal (a dc component). This is also applicable for *single dish* observations. In real life there is a loss in correlation for large

interferometers (Thompson 1982). For totally uncorrelated RFI, as for MERLIN, VLBA, and EVN, we find that
$\mathrm{rms}_{RFI} = \sqrt{P_{\mathrm{sys}}^2 + \beta(P_{RFI})^2}\frac{1}{\sqrt{M}}$
and
$G_{\mathrm{EXC}} = \sqrt{1+\beta\alpha^2}\sqrt{(1-\beta)}$.
The above formulae presume that the parts of the data containing RFI (βM) are completely excised. But sometimes this operation is not possible because of technical constraints in the existing hardware. The alternative then is to substitute these βM samples by noise-like numbers with a variance approximately the same as for the pure P_{sys}. Substitution by zeros is bad because of the undesirable shift in the output. In that case the rms and SNR after RFI excision are $\mathrm{rms}_{\mathrm{EXC}} = \frac{P_{\mathrm{sys}}}{\sqrt{M}}$, and $SNR_{\mathrm{EXC}} = \frac{P_{\mathrm{sig}}}{P_{\mathrm{sys}}}(1-\beta)\sqrt{M}$, which means that the astronomical signal is reduced by a factor $(1-\beta)$. Now let us consider the more realistic situation of non-ideal RFI detection and excision. There is always a delay before the RFI is detected (recognized), which could be considerable for a weak RFI. It is assumed that the probability distribution of the system noise in the $t \bigoplus f$-plane in the absence of RFI is Gaussian with a mean $\mu_0 = 0$ and a standard deviation (rms) of $\sigma = 1$. Let h be the one-sided normalized detection threshold, such that the probability of a false alarm is $p_{\mathrm{FA}} = 1 - \Phi(h, 0, 1)$, where $\Phi(x, \mu, \sigma)$ is the cumulative Gaussian distribution with a mean μ and a variance σ^2. The averaged run length (ARL or detection delay) in the absence of RFI is $ARL = 1/p_{\mathrm{FA}}$. In the presence of RFI a biasμ_{RFI} is introduced resulting in an ARL of $ARL = 1/(1 - \Phi(h, \mu_{RFI}, 1)), \mu_{RFI} = \mathcal{P}_{RFI}/\sigma$. The ARL in the presence of RFI corresponds to the number of RFI samples that go *unnoticed* by the detection procedure. All samples above the threshold are deleted, but those in the ARL regions remain. Thus the rms after RFI excision is

$$\mathrm{rms}_{\mathrm{EXC}} = \sqrt{\left(\frac{\mathcal{P}_{\mathrm{sys}}}{\sqrt{M(1-\beta p_{\mathrm{det}})}}\right)^2 + \beta(1-p_{\mathrm{det}})(\alpha\mathcal{P}_{\mathrm{sys}})^2},$$

and $p_{\mathrm{det}} = 1 - \Phi(h, \mu_{RFI}, 1)$. Until now only 100% correlated RFI has been considered (single dish or short-baseline radio interferometer). For uncorrelated RFI at the radio interferometer site, the impact of RFI is only in the growth of the total variance, that is

$$\mathrm{rms}_{\mathrm{EXC}} = \sqrt{\left(\frac{\mathcal{P}_{\mathrm{sys}}}{\sqrt{1-\beta p_{\mathrm{det}}}}\right)^2 + \beta(1-p_{\mathrm{det}})(\alpha\mathcal{P}_{\mathrm{sys}})^2}\frac{1}{\sqrt{M}}.$$

6.2. Excision using filtering techniques

The optimally expected gain for single-dish observations can be expressed as the SNR ratio of the total power detector (radiometer) output with a cleaning procedure (subtraction of RFI estimates) compared to the SNR without this subtraction:

$$G_{\mathrm{CLN}} = \frac{\left[(Q_1+Q_2)^2 - 2Q_1 - Q_2\right]^{1/2}(Q_1^2+Q_2)^{1/2}}{Q_1(Q_1+Q_2)}, \quad (7)$$

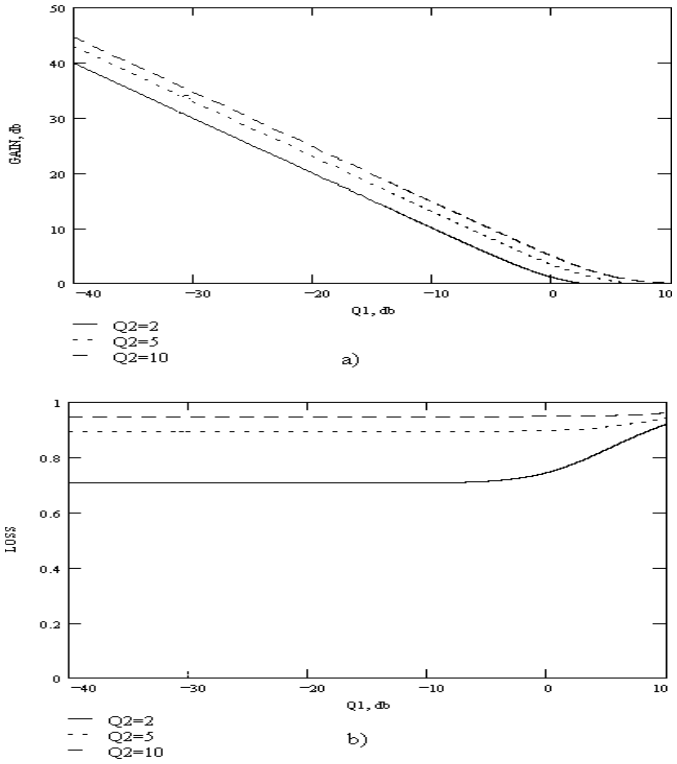

Fig. 19. The effectiveness of RFI suppression with filtering but without using a reference channel. The gain and loss are plotted using $Q_1 = \sigma_{\mathrm{sys}}^2/\sigma_{RFI}^2$ and $Q_2 = \Delta f/\Delta F_{RFI}$ as free parameters.

and the loss is expressed as the SNR after the application of CLEAN compared to the *ideal SNR* in the absence of RFI:

$$R_{\mathrm{CLN}} = \frac{\left[(Q_1+Q_2)^2 - 2Q_1 - Q_2\right]^{1/2}}{(Q_1+Q_2)}, \quad (8)$$

where $Q_1 = \sigma_{\mathrm{sys}}^2/\sigma_{RFI}^2, Q_2 = \Delta f/\Delta F_{RFI}$. These values of G_{CLN} and R_{CLN} give preliminary indication of the expected benefits in the optimal steady-state case. Figures 19a,b show how G and R depend on Q_1, while treating Q_2 as a free parameter. It is clear that for
$Q_1 \ll 1, G_{\mathrm{CLN}} \to \frac{Q_2^{1/2}}{Q_1}, R_{\mathrm{CLN}} \to 1$.
When $Q_2 \approx 1$, then $R_{\mathrm{CLN}} \to 0$ because both the wanted signal and the RFI have the same bandwidth and during an *autoclean* procedure the signal is subtracted from itself. Therefore, this RFI excision method is only useful when $Q_2 > 1$ for continuum observations. In the case of spectral-line observations, where the x_{RFI} occupies the same spectral region as the signal x_{sig} and $Q_2 \approx 1$, the RFI rejection should be done using a reference channel.

The more complicated case of a correlation interferometer will now be considered, where the RFI signals at both sites are not 100% correlated. ρ_{RFI} is the correlation coefficient between the RFI waveforms at the two sites. This ρ_{RFI} is a time-varying parameter ($0 < \rho_{RFI} < 1$), which depends on parameters as the distance between the antennas, the propagation effects, the pointing of the

antennas, the fringe stopping procedure, etc. The impact of the *RFI* is double-sided: it affects both the cross-correlation (cross-spectrum) bias and the growth of the variance. For a long-baseline interferometers such as the VLBI arrays and MERLIN, ρ_{RFI} is practically equal to zero and the main impact of the *RFI* is the growth of the variance. For the short-baseline correlation pairs of the WSRT or VLA, the bias of the mean becomes the most important distortion. The three formulas for estimating the processing benefits after *RFI* suppression using a filtering technique are expressed as:

$G_{\rm CLEAN}$ is the ratio of the SNR at the correlator output with the presence of *RFI* with cleaning and of the SNR with the presence of the *RFI* but without cleaning:

$$G_{\rm CLEAN}=\frac{(Q_1+Q_2)^2\sqrt{Q_1^2+2Q_1+Q_2+\rho^2Q_2}}{Q_1\sqrt{(Q_1+Q_2)^4-2Q_1^3-5Q_1^2Q_2-4Q_1Q_2^2-Q_2^3+\rho^2Q_2Q_1^2}}\,(9)$$

R_{CLEAN} is the ratio of the SNR at the correlator output with the presence of the *RFI* but with CLEAN and of the SNR without *RFI* (the ideal SNR):

$$R_{\rm CLEAN}=\frac{(Q_1^2+2Q_1Q_2+Q_2^2-2Q_1-Q_2)}{\sqrt{(Q_1+Q_2)^4-2Q_1^3-5Q_1^2Q_2-4Q_1Q_2^2-Q_2^3+\rho^2Q_2Q_1^2}}\quad(10)$$

$B_{\rm CLEAN}$ is the ratio of the bias at the correlator output with the presence of the *RFI* and with cleaning and of the bias with the presence of the *RFI* but without cleaning:

$$B_{\rm CLEAN}=\left(\frac{Q_1+Q_2}{Q_1}\right)^2.\qquad(11)$$

Figures 20a–c represent these characteristic parameters as a function of Q_1, while Q_2 is a free parameter. These filtering techniques, based on estimating the *RFI* and subsequently subtracting it from an input waveform (or its complex spectrum), represent a more generalized form of excision (blanking), In the case of a strong narrow-band this reduces to a bandstop (notch) filter or to a hard thresholding method in the temporal domain.

6.3. Adaptive cancellation using reference channels

For spectral line observations, where x_{RFI} occupies the same spectral region as the signal $x_{\rm sig}$ and $Q_2\approx 1$, the *RFI* rejection should be made with the aid of an auxiliary reference channel. Otherwise the useful coherent signal will be subtracted together with the *RFI*. The output of this auxiliary channel is described as:

$$y_{\rm aux}(t)=x_{\rm sys,aux}(t)+x_{RFI}(t)\star h(t),\qquad(12)$$

where $x_{\rm sys,a}(t)$ is the auxiliary channel system noise, $h(t)$ is the time transfer function of the auxiliary channel and $\star$ denotes convolution. We also have a description of the main channel:

$$y_{\rm main}(t)=x_{\rm sig}(t)+x_{\rm sys}(t)+x_{RFI}(t).\qquad(13)$$

The *RFI* estimate $\widehat{x_{RFI}(t)}$ is now obtained from $y_{\rm aux}(t)$. Formulas for gain and loss for single dish observations with

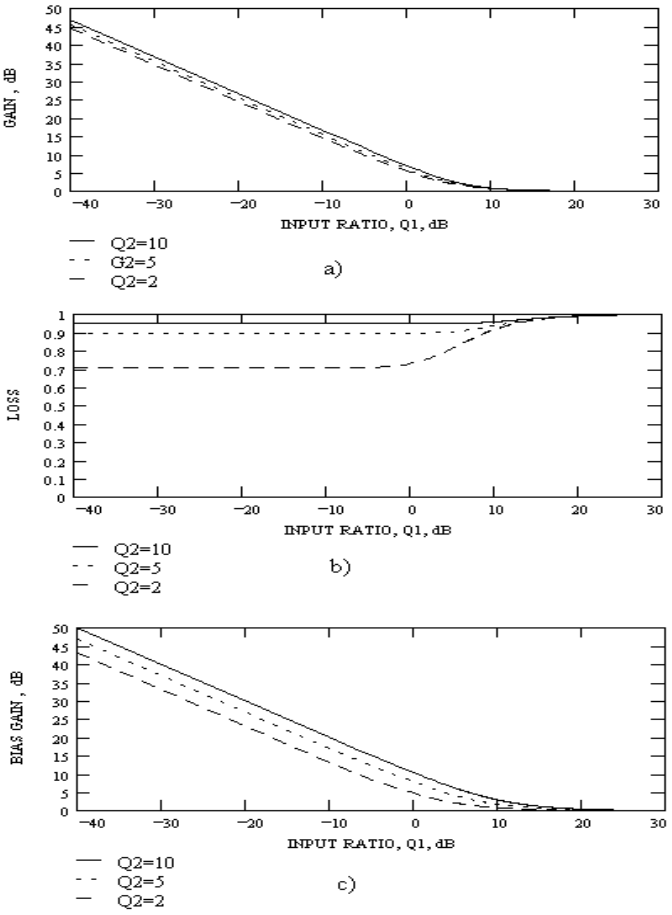

Fig. 20. The effectiveness of *RFI* suppression with filtering without a reference channel for a correlation interferometer. The gain, loss, and bias parameters are presented as functions of $Q_1=\sigma^2_{\rm sys}/\sigma^2_{RFI}$, while $Q_2=\Delta f/\Delta F_{RFI}$ is a free parameter.

$h(t)=\delta(0)$ are:

$$G_{\rm aux}=\frac{(Q_1^2+Q_2)^{1/2}(Q_a+Q_2)}{(Q_1^2Q_a^2+2Q_1^2Q_aQ_2+Q_1^2Q_2^2+Q_2Q_a^2)^{1/2}},\qquad(14)$$

and

$$R_{\rm aux}=\frac{Q_1(Q_a+Q_2)}{(Q_1^2Q_a^2+2Q_1^2Q_aQ_2+Q_1^2Q_2^2+Q_2Q_a^2)^{1/2}},\qquad(15)$$

where $Q_{\rm a}=\sigma^2_{\rm sys,a}/\sigma^2_{RFI}$. The situation is now rather different from the autoclean case without reference channel. Figure 21 shows the gain and loss parameters as a functions of Q_1 and $Q_{\rm a}$: (1) $Q_{\rm a}=-20$ dB, (2) $Q_{\rm a}=-30$ dB, (3) $Q_{\rm a}=-40$ dB. Besides $Q_2=1$ for Figs. 21a,b, $Q_2=5$ for Figs. 21c,d, and $Q_2=20$ for Figs. 21e,f. When $Q_1\ll 1$ and $Q_{\rm a}\ll 1$, again $G_{\rm aux}\to\frac{Q_2^{1/2}}{Q_1}$. When $Q_2\approx 1, Q_1\approx Q_{\rm a}$, and $R_{\rm aux}\to\sqrt{1/2}$, the *RFI* is deleted but the system noise of the auxiliary channel adds incoherently to the system noise of the main channel at the radiometer output. Figure 21 demonstrates the fact that it is necessary to provide $Q_{\rm a}\le Q_1$ for high precision *RFI* estimates in order to get the loss $R_{\rm aux}$ close to 1. For the two-antenna correlation interferometer with *RFI* suppression done at each site with the help of auxiliary channels, the formulas

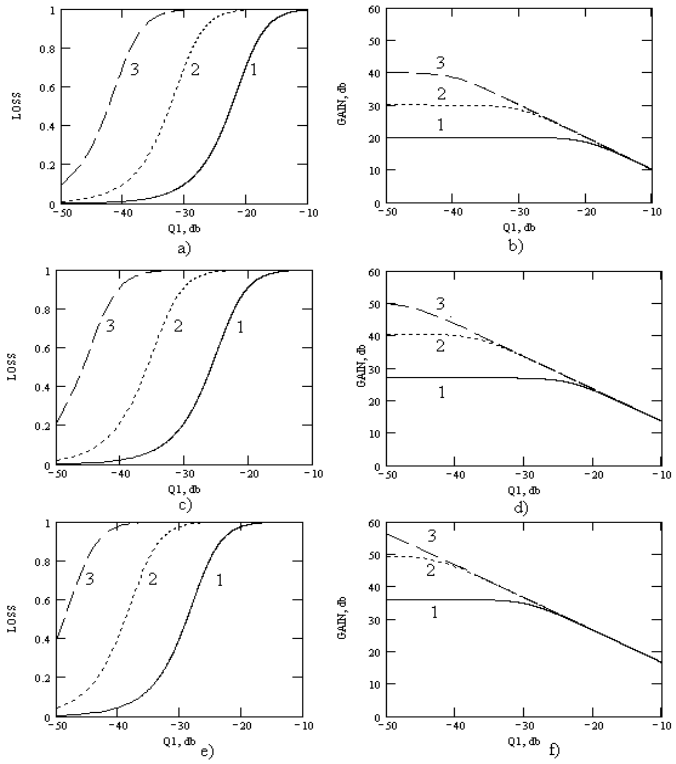

Fig. 21. The effectiveness of *RFI* suppression with a reference channel for single dish systems. The gain and loss are presented as functions of $Q_1 = \sigma^2_{\rm sys}/\sigma^2_{RFI}$ for three values for $Q_{\rm ref} = \sigma^2_{\rm sys,ref}/\sigma^2_{RFI}$: 1) −20 dB, 2) −30 dB, and 3) −40 dB, and for the following values for $Q_2 = \Delta f/\Delta F_{RFI} = 1$ for **a)** and **b)**, $Q_2 = 5$ for **c)** and **d)**, and $Q_2 = 20$ for **e)** and **f)**.

for gain and loss are as follows:
$G_{\rm cor} =$

$$\frac{(Q_{\rm a}+Q_2)\sqrt{Q_1^2+2Q_1+Q_2+\rho^2Q_2}}{\sqrt{Q_1^2Q_{\rm a}+2Q_1^2Q_{\rm a}Q_2+Q_1^2Q_2^2+2Q_{\rm a}^2Q_1+2Q_{\rm a}Q_1Q_2+Q_2Q_{\rm a}^2+\rho^2Q_2Q_{\rm a}}}, \tag{16}$$

and $R_{\rm cor} =$

$$\frac{Q_1(Q_{\rm a}+Q_2)}{\sqrt{Q_1^2Q_{\rm a}+2Q_1^2Q_{\rm a}Q_2+Q_1^2Q_2^2+2Q_{\rm a}^2Q_1+2Q_{\rm a}Q_1Q_2+Q_2Q_{\rm a}^2+\rho^2Q_2Q_{\rm a}}}, \tag{17}$$

where ρ is the correlation coefficient between the *RFI* at both sites. It is assumed here for simplicity that the *SNR*s of the *RFI* in the auxiliary channels are equal $Q_{1,\rm a} = Q_{2,\rm a} = Q_{\rm a}$, and that for the main channels $Q_{1,1} = Q_{1,2} = Q$. If the *RFI* is correlated at both sites, the false correlation will result in a bias and the gain after *RFI* suppression becomes:

$$B_{\rm cor} = \frac{Q_{\rm a}+Q_2}{Q_{\rm a}}. \tag{18}$$

Figure 22 shows $G_{\rm cor}, R_{\rm cor}$, and $B_{\rm cor}$ as a functions of Q_1 for the *RFI* input in the main channels, for $Q_2 = 1$, with $Q_{\rm a}$ having three values: (1) −20 dB, (2) −30 dB, and (3) −40 dB, and with $\rho = 1$. This Fig. 22 may be used to estimate how *RFI* suppression depends on

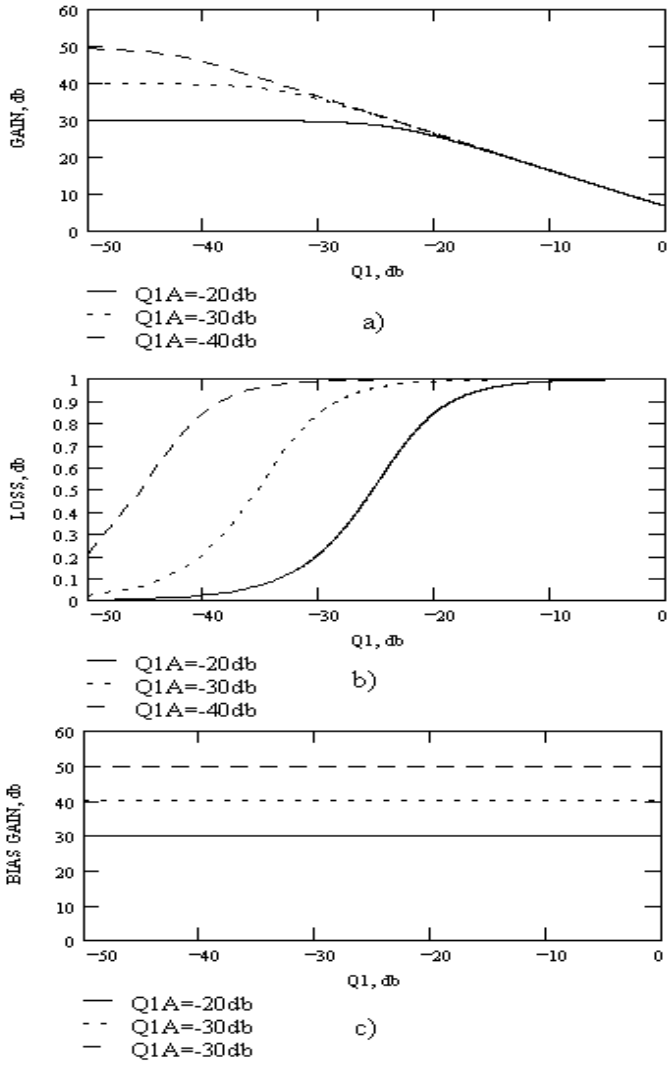

Fig. 22. The effectiveness of *RFI* suppression with a reference channel for the case of a correlation interferometer. The gain, loss, and bias are presented as a functions of $Q_1 = \sigma^2_{\rm sys}/\sigma^2_{RFI}$, of $Q_{\rm A} = \sigma^2_{\rm sys,ref}/\sigma^2_{RFI}$ for three values, for $Q_2 = \Delta f/\Delta f_{RFI} = 1$, and for $\rho = 1$.

$Q_{\rm a}$. However, in real-life $Q_{\rm a}$ increases and decreases together with Q_1, because the power of the *RFI* behaves more or less the same in the main and auxiliary channels. Therefore, Fig. 23 presents the same dependences as for Figs. 22, except that the value of $Q_{\rm a}$ is now proportional to $Q_{\rm a} = kQ_1$, with values for $k = 5$, 1.0, and 0.2. The lower the value of k, the better the auxiliary channel behaves, and the more effective the *RFI* suppression is.

6.4. Spatial filtering with multi-element systems

Adaptive nulling is an attractive possibility for multi-element radio interferometric radio telescopes. In order to get a rough estimate of the gains and losses for this type of *RFI* suppression, we use a simplified approach based on the block diagram of Fig. 24. All processing in the block diagram is made in the frequency domain after the Fourier transform, which is not shown in the diagram

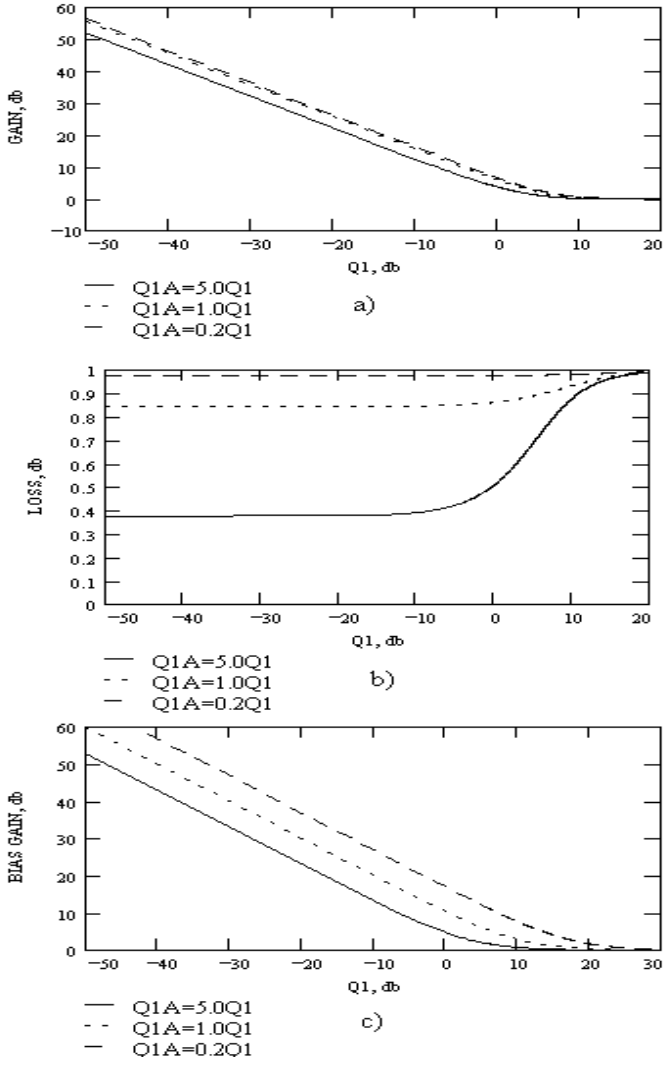

Fig. 23. The effectiveness of RFI suppression with reference channel for a correlation interferometer. The gain, loss, and bias are presented as a function of $Q_1 = \sigma^2_{\rm sys}/\sigma^2_{RFI}$, for three values of $Q_{\rm A} = \sigma^2_{\rm sys,ref}/\sigma^2_{RFI}$ proportional to Q_1, and for $Q_2 = \Delta f/\Delta f_{RFI} = 1$, and $\rho = 1$.

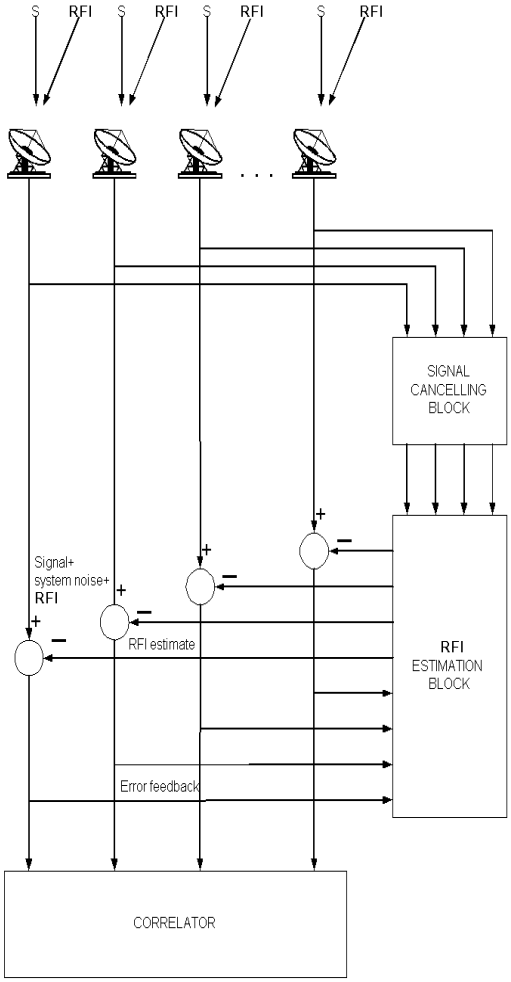

Fig. 24. A block diagram of the spatial filtering process for RFI suppression.

itself. In the following we consider a narrow-band situation. Signals from M antennas are supplied to the *signal cancelling block*, which serves to combine the antenna's signals in order to minimize the signal at the output of this block. This is done to prevent further degradation of the useful signals during the RFI suppression process. This is possible because the direction of arrival (DOA) of a wanted signal is known (prescribed). The outputs of the signal-cancelling block are processed in the *RFI-estimation block* in order to obtain estimates of the RFI signals, which will later be subtracted from the main antenna's signals and must provide minimal error signals after subtraction.

The algorithm inside the RFI-estimation block is not specific at this point. An adaptive algorithm is needed here, which can be a method of running estimates of the co-variation matrix, the LMS algorithm, or something else. The advantage of the procedure in this block diagram lies in keeping the amplitude and phase structure of the signal-of-interest intact. The subtraction of an RFI-estimate should not affect the wanted radio signal, and there is no need to do special bookkeeping of the complex adaptation coefficients used in the RFI-estimation block. The outputs of subtractor blocks are supplied to the correlator. Delay compensation is expected to happen inside the correlator block and fringe stopping is done before the subtractors. Let us consider a linear array with a distance between M elements equal to d working at a wavelength λ. A coherent plain-wave signal with the same amplitude S arrives at the array at an angle θ_S, resulting in the same system noise variance σ^2 for all receivers. In addition, there is a plain-wave RFI signal coming in from the direction θ_{RFI} with a uniform amplitude R for all antennas. So the array signal vector is described as

$$\boldsymbol{S} = S[1 \ \mathrm{e}^{-ja} \ \mathrm{e}^{-j2a} \ \ldots \ \mathrm{e}^{-jMa}]^T, \tag{19}$$

where $a = 2\pi d \sin(\theta_S)/\lambda$. The RFI vector is written as

$$\boldsymbol{RFI} = R[1 \ \mathrm{e}^{-jb} \ \mathrm{e}^{-j2b} \ \ldots \ \mathrm{e}^{-jMb}]^T, \tag{20}$$

where $b = 2\pi d \sin(\theta_{RFI})/\lambda$. Optimizing with weights may provide a maximum signal-to-noise ratio at the additive

output of the array $y(f)$ at frequency $f = c/\lambda$. This output is a linear combination of the input signals
$x_k(f) = S_k(f, \theta_S) + RFI_k(f, \theta_{RFI}) + n_k(f)$
such that

$$y(f) = \sum_{k=1}^{M} x(f)\overline{W}_{\mathrm{opt},k}(f), \tag{21}$$

or in vector form

$$\boldsymbol{y} = \boldsymbol{X}^T\overline{\boldsymbol{W}}_{\mathrm{opt}}. \tag{22}$$

The formalism of Minimum Variance Distortionless Response (MDVR, Haykin 1996, Ch. 5) for the beamformer protocol is then given by

$$\boldsymbol{W}_{\mathrm{opt}} = \boldsymbol{R}^{-1}\boldsymbol{S}(\theta_S)[\boldsymbol{S}^H(\theta_S)\boldsymbol{R}^{-1}\boldsymbol{S}(\theta_S)]^{-1}, \tag{23}$$

where the input $(M \times M)$ correlation matrix $\boldsymbol{R}$ for a weak signal ($S^2 \ll \sigma^2$) is expressed as:

$$\boldsymbol{R} = \boldsymbol{R}_n + \boldsymbol{R}_{RFI}(\theta_{RFI}), \tag{24}$$

$$\boldsymbol{R}_n = \begin{pmatrix} \sigma^2 & 0 & ... & 0 \\ 0 & \sigma^2 & 0 & 0 \\ ... & ... & ... & ... \\ 0 & 0 & 0 & \sigma^2 \end{pmatrix}, \text{and} \tag{25}$$

$$\boldsymbol{R}_{RFI} = RFI \cdot RFI^H. \tag{26}$$

The superscript H denotes here an Hermitian transposition (actually transposition combined with complex conjugation). The variable f will be omitted from now on because all results will be valid for a certain frequency f.

Before the formation of $\boldsymbol{W}$ a signal cancelling component $(M-1)\times M$ matrix $\boldsymbol{C}$ is introduced, which is written as:

$$\boldsymbol{C} = \begin{pmatrix} -1 & -1 & -1 & -1 \\ S_2 & 0 & 0 & 0 \\ 0 & S_3 & 0 & 0 \\ ... & ... & ... & ... \\ 0 & 0 & 0 & S_M \end{pmatrix}, \tag{27}$$

The optimal weights then become:

$$\boldsymbol{W}_{\mathrm{opt,ca}} = (\boldsymbol{C}^H\boldsymbol{R}\boldsymbol{C})^{-1}\boldsymbol{C}^H\boldsymbol{R}[\boldsymbol{S}(\boldsymbol{S}^H\boldsymbol{S})^{-1}]. \tag{28}$$

The array output is then written as

$$y = \boldsymbol{X}^T\boldsymbol{W}_0^H - \boldsymbol{X}^T\boldsymbol{W}_{\mathrm{opt,ca}}^H, \tag{29}$$

where $\boldsymbol{W}_0 = \boldsymbol{S}(\boldsymbol{S}^H\boldsymbol{S})^{-1}$ is the steering vector corresponding to the direction-of-arrival of the signal-of-interest θ_S, which is also called the fringe stopping for radio astronomy arrays. At this point the array output values can be calculated as follows:
a) the power for the signal-of-interest is

$$P_S = \boldsymbol{W}_0^H\boldsymbol{R}_S\boldsymbol{W}_0, \tag{30}$$

$$\text{where} \quad \boldsymbol{R}_S = \boldsymbol{S}\boldsymbol{S}^H, \tag{31}$$

b) the power of the RFI at the array output is

$$P_{RFI} = \boldsymbol{W}_{\mathrm{opt,ca}}^H\boldsymbol{R}_{RFI}\boldsymbol{W}_{\mathrm{opt,ca}}, \tag{32}$$

and c) the total power of noise-plus-RFI with the optimal processing is

$$P_{n+RFI} = \boldsymbol{W}_{\mathrm{opt,ca}}^H\boldsymbol{R}\boldsymbol{W}_{\mathrm{opt,ca}}, \tag{33}$$

while the total power of noise-plus-RFI without the optimization processing is

$$P_{n+RFI,0} = \mathbf{W}_0^H\boldsymbol{R}\boldsymbol{W}_0 \tag{34}$$

Using these values, the signal-to-interference-plus-noise ratio ($SINR$), and hence the gain and loss after optimisation processing are as follows:

$$G = \frac{SINR_{\mathrm{output}}}{SINR_0} = \frac{P_S/P_{n+RFI}}{P_S/P_{n+RFI,0}} = \frac{P_{n+RFI,0}}{P_{n+RFI}}, \tag{35}$$

a) the loss is

$$L = \frac{SINR_{\mathrm{output}}}{P_S/P_n} = \frac{P_n}{P_{n+RFI}}, \tag{36}$$

b) and the interference-to-noise ratio (INR) is

$$INR_{\mathrm{output}} = \frac{P_{RFI}}{\boldsymbol{W}_{\mathrm{opt,ca}}^H\boldsymbol{R}_n\boldsymbol{W}_{\mathrm{opt,ca}}}. \tag{37}$$

These results may now be applied to an array example with $d = 10(\lambda/2)$ and $\lambda = 21$ cm for $\sigma^2 = 1$. Figures 25–28 show the power pattern for the array, the output INR, the gain, and the loss, respectively. These parameters are presented as a function of the angle between the DOA's of the signal-of-interest and of the RFI. It is clear that there are some periodic angular domains, where substantial losses occur in the vicinity of the grating lobes: the useful signal and the RFI are "in-phase" at these angles and it is impossible to decouple them. Figure 29 represents the output INR versus the input INR for different numbers of antennas $M = 16$, 6, and 2. The INR value does not provide the complete answer on the question of benefits of the RFI suppression, but it is sometimes used for this purpose. Figure 29 also illustrates the fact that the algorithm does not recognize weak RFI at values below ≈ -10 dB for $M = 16$.

All these figures have been given here for illustrative purposes, in order to describe the effects for a sparse periodic array. Real arrays have much larger inter-element distances and are not so regular (except for the WSRT). Therefore, the expected values for the gain and the loss should be calculated for the particular array-source-RFI geometry and for a particular RFI intensity. The RFI signals also enter the frontend through the antenna sidelobes and the sources are often situated in the near-field zone of the antenna. Therefore, the scenario described above might indeed be too idealized.

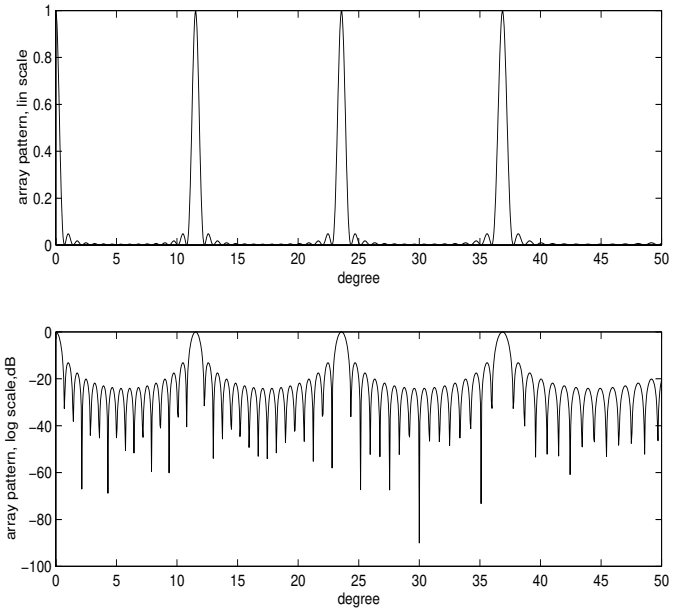

Fig. 25. The power pattern of a 16-element array with interval between elements of $10\lambda/2$ and for $\lambda = 21$ cm.

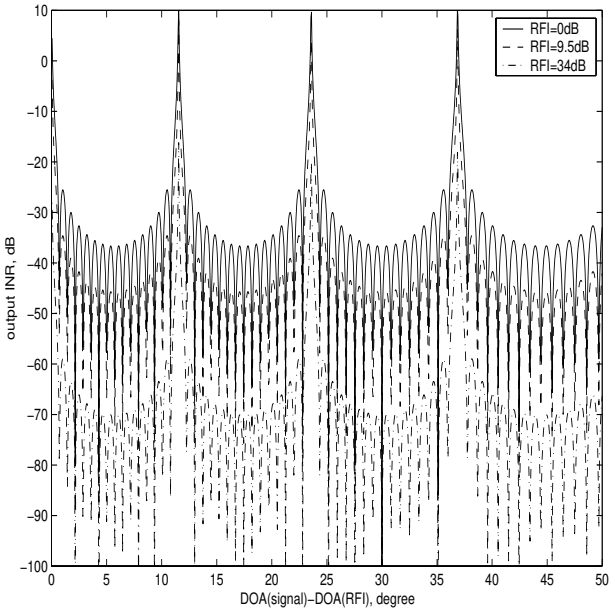

Fig. 26. The output interference-to-noise ratio for a 16-element array at regular intervals of $10\lambda/2$ for $\lambda = 21$ cm, versus the angle between the DOA of the signal-of-interest and RFI. The free parameter is the relative input RFI intensity $P_{RFI}/P_{\rm sys}$.

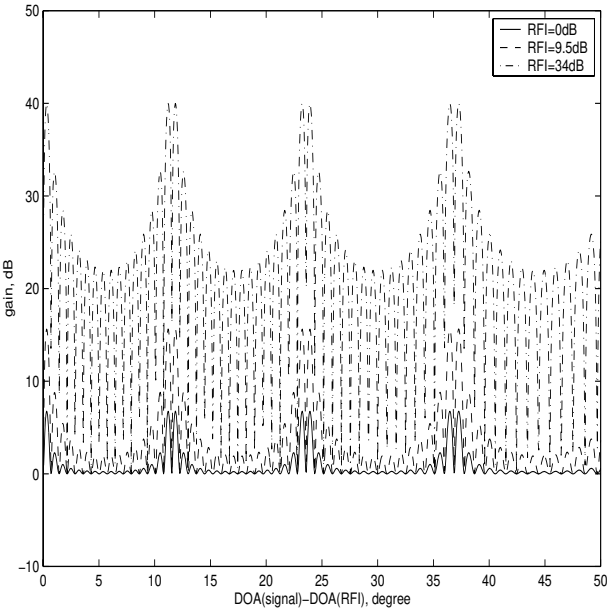

Fig. 27. The output gain after RFI suppression for a 16-element array at regular intervals of $10\lambda/2$ for $\lambda = 21$ cm, versus the angle between the DOA of the signal-of-interest and RFI. The free parameter is the relative input RFI intensity $P_{RFI}/P_{\rm sys}$.

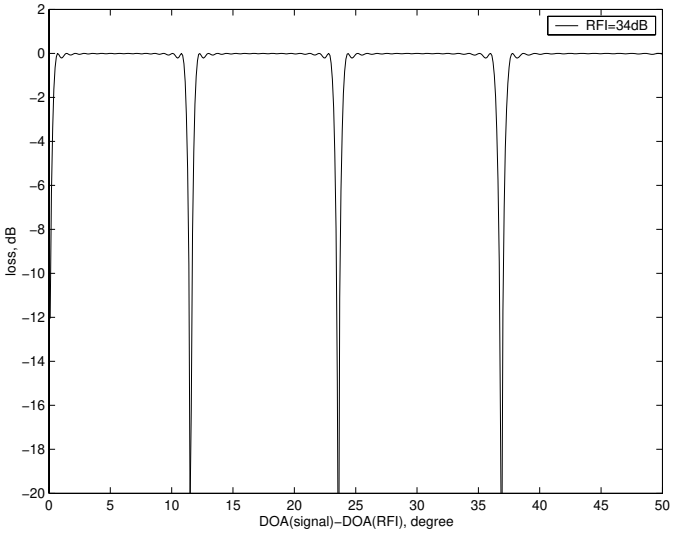

Fig. 28. The output loss after RFI suppression for a 16-element array at regular intervals of $10\lambda/2$ for $\lambda = 21$ cm, versus the angle between the signal of interest and RFI directions of arrival. The relative input RFI intensity $P_{RFI}/P_{\rm sys} = 34$ dB.

6.5. Excision using the probability distribution analysis of the power spectrum

Practically obtainable statistical errors with this method depend on the fitting procedure used to determine the estimate of the power spectrum $P(f)$. There are several approaches to do this: a) to calculate a histogram $\widehat{W}[P(f)]$ or a sample probability distribution of $P(f)$, or b) to sample the statistical moments $\widehat{\mu}_i[P(f)]$. For the case of *histogram fitting*, the values at each frequency bin f can be used to make estimates of the system-plus-signal noise rms $\widehat{\sigma}$, and the interference amplitude $\widehat{A}$, in order to minimize the residuals, such that:

$$\widehat{\sigma}, \widehat{A} : \max(\widehat{W}[P(f)] - W[P(f, \widehat{\sigma}, \widehat{A})]) \rightarrow \min . \qquad (38)$$

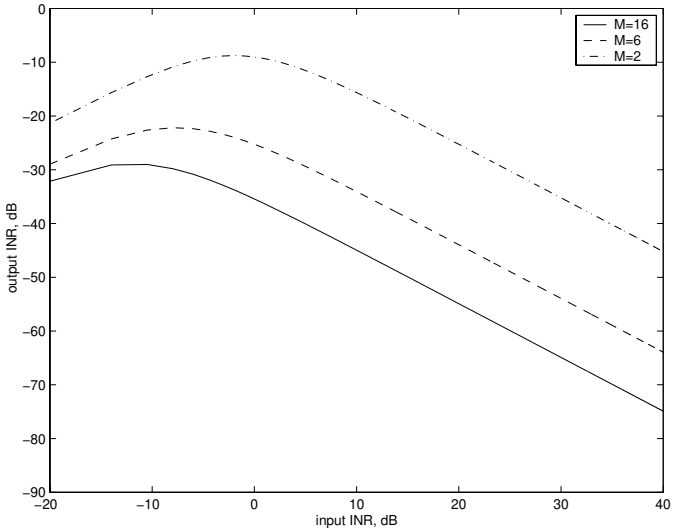

Fig. 29. The output interference-to-noise ratio (INR) after RFI suppression for an array at regular intervals of $10\lambda/2$ for $\lambda = 21$ cm, versus the input INR. The angle between the DOA of the signal-of-interest and the RFI is 20°. The free parameter is the number of antennas in the array.

After the moment fitting procedure, we find

$$\widehat{\sigma}, \widehat{A} : (\widehat{\mu}_i[P(f)] - \mu_i[P(f, \widehat{\sigma}, \widehat{A})])^2 \rightarrow \min, \qquad (39)$$

where $W[P(f, \sigma, A)]$ and $\mu_i[P(f, \sigma, A)]$ are the theoretical non-central χ^2 probability distribution and its central moments, respectively. This fitting is a non-linear procedure and the post-processing gain depends on the input interference-to-noise ratio $INR_{\rm input}$ in a complex way. For large $INR_{\rm input}$, the gain can be estimated approximately as $10\log(INR_{\rm input}) + 5\log(M)$, where M is the number of averaged spectra.

The effectiveness of this method depends also on the temporal stability of INR. Equations (38) and (39) must be solved under the assumption of a constant RFI signal during averaging, so that the total averaging procedure can be divided in the following stages: preliminary averaging – RFI subtraction – final averaging.

References

Ardenne van, A., Smolders, B., & Hampson, G. 2000, Proc. SPIE, 4015, 420

Barnbaum, C., & Bradley, R. F. 1998, AJ, 115, 2598

Basseville, M., & Nikiforov, I. V. 1993, Detection of Abrupt Changes: Theory and Application (Prentice Hall: Englewood Cliffs, New Jersey)

Bregman, J. D., Proc. SPIE, 4015, 19

Briggs, F. H., Bell, J. F., & Kesteven, M. J. 2000, AJ, 120, 3351.

Cohen, J. 1999, Astr. Geoph., 40, 6

RAF (Committee on Radio Astronomy Frequencies), 1997, Handbook for Radio Astronomy, (ESF: Strassburg)

Ellington, S. W., Bunton, J. D., & Bell, J. F. 2000, Proc. SPIE, 4015, 400

Fridman, P. A. 1996, Proc. IEEE Workshop on Statistical Signal and Array Processing, Corfu, 264

Fridman, P. A., & Berlin, A. B. 1996, Proc. XXV URSI GA (URSI, Gent), 750

Fridman, P. A. 1997, NFRA Note 664 (NFRA: Dwingeloo)

Fridman, P. A. 2001, A&A, 368, 369

Galt, J. 1990, Nature, 345, 483

Haykin, S. 1996, Adaptive Filter Theory, Chapter 5 (Prentice Hall, N.J.)

Kahlmann, H. C. 1999, Review of Radio Science 1996–1999, ed. W. Ross Stone (URSI: Oxford University Press), 751

Leshem, A., van der Veen, A. J., & Boonstra, A.-J. 2000, ApJ, 131, 355

Lemmon, J. J. 1997, Radio Sci., 32, 525

Maddox, J. 1995, Nature, 378, 11

Middleton, D. 1972, Trans. IEEE EMC, EMC-14 , 38

Middleton, D. 1977, Trans. IEEE EMC, EMC-19, 106

Moran, J. M. 1995, in Very Long Baseline Interferometry and VLBA, ed. J. A. Zensus, P. J. Diamond, & P. J. Napier (ASP, San Francisco), 181

Pankonin, V., & Price, R. M. 1981, Trans. IEEE EMC, 23, 308

Spoelstra, T. A. Th. 1997, Tijdschrift van het Nederlands Elektronica- en Radiogenootschap, 62, 13

Thompson, A. R. 1982, Trans. IEEE AP, 30(3), 450

Waterman, P. J. 1984, Trans. IEEE EMC, 26, 29

Weber, R., Faye, C., Biraud, F., & Dansou, J. 1997, A&AS, 126, 161

Widrow, B., & Stearns, S. 1985, Adaptive Signal Processing (Prentice-Hall: Englewood Cliffs)